Antimicrobial Cellulose Nanocrystals Containing Quaternary Ammonium Polymers Prepared via Atom Transfer Radical Polymerization

by

Lian Han

A thesis

presented to the University of Waterloo

in fulfillment of the

thesis requirement for the degree of

Master of Applied Science

in

Chemical Engineering

Waterloo, Ontario, Canada, 2020

Author's Declaration

I hereby declare that I am the sole author of this thesis. This is a true copy of the thesis, including any required final revisions, as accepted by my examiners.

I understand that my thesis may be made electronically available to the public.

Abstract

Nanomaterials have been widely used as antimicrobial agents for their high efficiency. However, the lack of recovery techniques and toxicity has raised concerns for the use of these materials. Cellulose nanocrystals (CNCs), extracted from plants and agriculture biomass via acid hydrolysis possess many unique features, such as high mechanical strength, high aspect ratio, excellent colloidal stability, and biocompatibility. With the growing interests in green chemistry and chemical process, the modification and utilization of CNCs has appealed to more scientists and researchers.

In this study, a CNCs based antimicrobial nanomaterials was developed by grafting poly(diethylaminoethyl methacrylate) (PDMAEMA) via surface-initiated ARGET-ATRP and quaternizing the grafted polymer. The grafting density and molecular weight of the PDMAEMA-g-CNC was controlled by adjusting the surface initiator immobilization and monomer concentration. The degree of quaternization of different PDMAEMA-g-CNCs with various grafting density and chain length were evaluated, and the antimicrobial activity was tested. It is found that the types of quaternizing agents, grafting density, and polymer chain length could affect the surface charge, morphology, degree of quaternization, and antimicrobial activity of CNCs. The smaller quaternizing agents, lower chain density and longer chain length could lead to higher degree of quaternization and enhance the antimicrobial activity of the Q(PDMAEMA)-g-CNC. These findings could be applied to optimize the CNC ATRP surface grafting systems and could be potentially used in applications, such as Pickering emulsion, antimicrobial and drug delivery.

Acknowledgments

First and foremost, I would like to thank to my supervisor Dr. Michael K. C. Tam for giving me the opportunity to join his research group to pursue my master's degree. With my deepest respect, I want to thank him for not only the guidance and help with my research, but also the helpful advice and experiences towards my personal development. I am truly grateful for all the resources he provided me to conduct my master's research, and the guidance and support he offered me in difficult times. I would not have accomplished all the goals and achievements without his help. Everything I learnt from him will be my precious experience for my lifetime.

Also, I would like to thank all the members in Tam's research group for their support and kindness. I would like to thank Dr. Nate Grishkewich for his generous help and support as a research colleague and wonderful friend. Every time I encountered difficulties, he always helps without hesitation. He is always patient and willing to listen to me about my thoughts and emotions whenever I was in need. I also would like to thank Dr. Mohankandhasamy Ram for working together with me and teaching me about biology experiments, which contributes a lot to this thesis. I would like to thank Dr. Rasool Nasseri Pourtakalo and Christopher Dutchman for inviting me to co-author a review paper. I would like to thank Dae Sung Kim for being such a great friend and helped with my paper. I would like to thank Weinan Zhao and Nadeem Akhtar for their support. I would like to thank co-op students Songbo Cui and Haoyu Zhang for their cooperation in electronic-skin projects. It was nice to work with them and I also learnt from them. Again, I would like to thank all the group members, it is my pleasure to work with you.

Special thanks to Dr. Houyong Yu for teaching and pushing me all the time during his visit. He always encourages me and shares his own research experience with me, his humble and hard-working really influences me a lot. I also want to thank him for teaching me in academic writing and offering the chance to collaborate with his research group. Special thanks to Dr. Yingzhan Li for his help and guidance in the lab, I learnt lots of experimental skills and writing skills from him. I also appreciate it that he often invited me for meals. I hope he can make great achievements in his future research.

Last but not least, I would like to thank my parents for their love and support. They are the most important people in my life, and I always appreciate their love and caring during my time in Canada. I feel sorry for the absence of new year for the past four years and I hope you can always stay healthy and happy. I would like to thank and give my deepest memory to my grandfather, who passed away during my study. I know you love me and have always been proud of me.

Table of Contents

List of Figures

List of Tables

Chapter 1 Introduction

1.1 Research overview

Nanomaterials have unique properties, such as high surface energy and mechanical strength, which has been utilized to fabricate antimicrobial materials with strong biocidal activity. However, many of these antimicrobial nanomaterials lack biocompatibility and show long-term environmental impact. Cellulose nanocrystals (CNCs) are extracted from natural cellulose by acid hydrolysis and have many unique features, such as high mechanical strength, high aspect ratio, excellent colloidal stability, and biocompatibility. With the growing interests in green chemistry and chemical process, it is of great research potential to develop a CNCs-based antimicrobial nanomaterials with high efficiency and low environmental impact.

There are two major objectives of this research: 1) Develop quaternary ammonium-modified cellulose nanocrystals (QA-CNCs) and explore its potential as antimicrobial nanomaterials, 2) Investigate and optimize the factors that can enhance the antimicrobial activity of the QA-CNC systems.

1.2 Methodology

This thesis focuses on developing an antimicrobial CNCs system by surface grafting of antimicrobial polymer with cationic quaternary ammonium groups. Surface-initiated Activator Re-Generated by Electron Transfer Atom Transfer Radical Polymerization SI-(ARGET) ATRP was used to graft PDMAEMA from the CNC surface. The grafting density, molecular weight can be controlled by changing the reaction conditions. After polymer grafting, the grafted CNCs was quaternized using

different quaternizing agents and tested for the degree of quaternization via titration. Finally, the antimicrobial efficiency was evaluated with yeast tests and antibacterial tests.

1.3 Research outline

Chapter 1

In this chapter, a research overview and the research objectives are described, and the methodology and research outline of this thesis is presented.

Chapter 2

In this chapter, a comprehensive literature review was conducted. The contents include three parts: 1) an introduction to nanotechnology and antimicrobial nanomaterials, the synthesis, development, and working aspects of common antimicrobial nanoparticles. 2) a review on CNCs, the development, extracting methods, physical properties, surface chemistry and modifications of CNCs. 3) an introduction to the development, mechanism, and the utilization of quaternary ammonium compounds in antimicrobial applications.

Chapter 3

In this chapter, the synthesis, quaternization using different materials, and the factors that can modulate the antimicrobial activity of PDMAEMA-g-CNCs are discussed. The chemical reaction, morphology, surface charge and colloidal stability, degree of quaternization, and antimicrobial activity were studied. By comparing the surface charge and titration results, the best quaternizing agent was chosen to achieve a

maximum degree of quaternization. The antimicrobial tests were conducted, and the problems and potential approach of optimizing this Q(PDMAEMA)-g-CNC system was discussed.

Chapter 4

In this chapter, the control of polymer grafting density, chain length, and its effects on quaternization and antimicrobial activity are discussed. The morphology, surface charge, degree of quaternization and antimicrobial activity of four PDMAEMA-g-CNCs with different chain densities and chain lengths were studied. The principles behind the effects of chain density and chain length on degree of quaternization (DQ) and antimicrobial activity were discussed.

Chapter 5

This chapter provides a summary of the research conducted and describes possible issues to be addressed in the future.

Chapter 2 Literature Review

2.1 Introduction to nanotechnology and antimicrobial nanomaterials

2.1.1 Nanotechnology and nanomaterials

Nanotechnology is an interdisciplinary filed that focuses on materials or composites with dimensions in nano range. Nanomaterials and nanocomposites possess unique physical or chemical properties due to their high surface energy, which enables novel designs and applications of existing materials. The principles of nanotechnology were introduced to agriculture, food industry, water treatment, health care, energy, and electrical engineering.[1-13] As the result of growing research on nanotechnology, there were more than 189,000 international patents in the field of nanotechnology and nanoproducts by 2017. It was estimated that the global nanotechnology market size was between 45 billion to 50 billion USD as of 2018, with a compound annual growth rate (CAGR) of 13% during the forecast period of 2019 to 2025.[10] Among these growing market in nanotechnology, biomedicine and health care are among the most important field of application. Recent nanotechnology research on biomedicine includes applications in quantum dots-incorporated bio-imaging,[1] thermal therapy and radiation therapy,[12, 14] nanomaterials for biosensing,[9, 15, 16] drug delivery nanocomposite systems.[17, 18] These novel designs of nanomaterials and nanocomposites revealed the great potential of nanotechnology in health care and biomedical engineering. Therefore, further research and discussion in this area are important and necessary.

2.1.2 Development of antimicrobial nanoparticles

Silver has a long history of being used to produce potable water and has been used for burns and wound dressing for centuries.[19] Silver metal and its compound have been found to have strong broad-spectrum antimicrobial activity due to the silver ions, which are known to interact with bacterial cell and inhibit its growth in a number of different ways: binding with thiol groups of proteins and enzymes to disrupt bacterial respiration and substance transport, interacting with cell wall and membrane to damage the function of cell membrane, and affecting nucleic acid to destroy bacterial cellular activities.[20-24] The antimicrobial efficiency of bulk silver and silver compound is determined by the release rate of silver ion, however the high cost of silver metal further limited the use of these materials as antimicrobial agents.

With the development of nanotechnology and nanomaterials, a new form of silver antimicrobial materials , i.e. silver nanoparticles (NPs) have attracted new interest.[19, 21, 24, 25] The size of silver NPs varies from 10 and 80 nanometers and display much higher antimicrobial efficiency, with minimal inhibitory concentrations (MIC) down to tens of μg/mL level, compared to bulk metallic silver.[21] It is suggested that the smaller size of silver NPs resulted in the higher surface energy and rate of silver ion release, which promotes the lethal interactions with micro-organisms leading to higher antimicrobial efficiency.[19, 21, 22, 24, 25] The successful research outcomes using silver NPs generated increasing interests as antimicrobial nanomaterials.

There has been a tremendous growth in research on antimicrobial NPs since the discovery of silver NPs. Various types of antimicrobial NPs have been developed, which can be classified into three major categories: inorganic NPs, organic NPs, and hybrid

NPs. (Fig. 2-1) Common inorganic NPs include metallic nanoparticles, such as silver NPs and gold NPs,[19, 21, 25-27] metal oxides such as TiO_2 and ZnO,[28-32] and other ion doped metal oxides and insoluble metal salts.[33-35] These nanoparticles occur in different shapes, such as nanospheres, nanorods, nanoplates, and nanoflowers.[36-40] Organic NPs usually refer to organic compounds NPs such as curcumin, polymer NPs and their derivatives.[41-45] Hybrid NPs consist inorganic NPs or metal ions and organic materials, usually polymers, such as NPs incorporates nanofibers, surface modified metal NPs, and polymer-metal ions complex.[46-50]

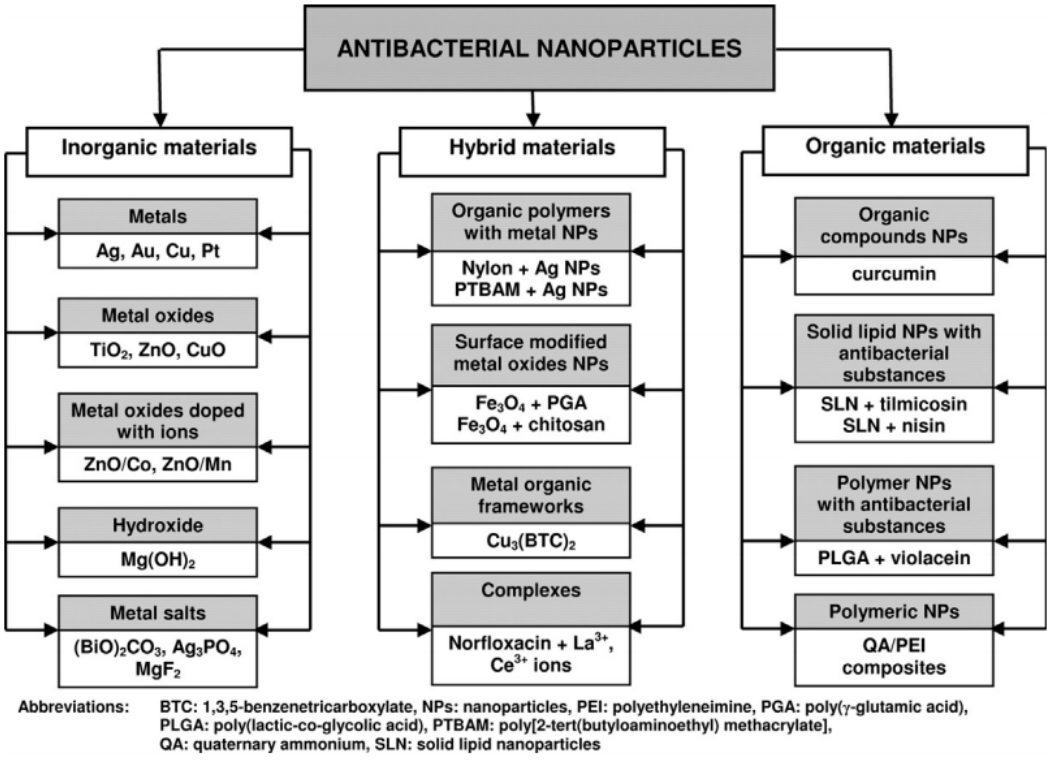

Figure 2-1 Antibacterial nanoparticles categorized by material type. (Adapted from Morizt et al.[51])

The general preparation methods of these nanoparticles follow one of the two methods: 1) physicochemical method, and 2) biological method. Physicochemical method is the most common synthesis approach for metallic NPs. Evaporation/ condensation method is a straightforward method for NPs synthesis. For example, Ayesh et al. reported on the synthesis process of titanium NPs by inert gas condensation.[52] The titanium nanoclusters were generated in an ultra-high vacuum system that controls the size of NPs with inert gas flow, aggregation region, and sputtering discharge power. Despite the fact that physical condensation can easily control the chemical composition of NPs, the high vacuum and power consumption limits its application as a commercial method. Currently, most NPs are prepared by reducing suitable metal ions using reducing agents, such as sodium borohydride, ascorbates, or citrates.[19, 24, 25, 51, 53] During the synthesize process, one or more capping agents are often introduced to control the growth and size of NPs and enhance stability.[26, 28] For example, Chen et al. compared the size distribution of gold NPs in the absence/presence of 1-dodecanethiol (DDT) capping agent.[54] The diameter of gold NPs ranged from 2-16 nm without DDT while the thiol-capped NPs had a narrow diameter distribution of around 5.6 nm. Although antimicrobial NPs prepared by conventional physicochemical method is simple and controllable, the use of toxic reducing agents, such as sodium borohydride and organic solvents pose environmental issues and potential health risks, especially for biomedical applications.[27, 30, 55]

In order to address these challenges, there is a need to develop non-toxic, environmental-friendly biosynthesis methods for antimicrobial NPs. Recent studies have focused on the biosynthesis of NPs using various plant extracts and microbial metabolism

activities.[27, 30-33, 40, 55-57] For example, lignin, a common biopolymer produced in pulping industry, were used to synthesize silver NPs as both a reducing and capping agent, where the size and distribution of silver NPs were controlled by lignin concentration in the process.[58] Also, the biosynthesis of copper/ copper oxide NPs using living bacteria or bacterial extracts were reported.[32, 55] These novel approaches of synthesizing NPs shows the future trend of making and applying antimicrobial nanomaterials.

2.1.3 Working mechanism of antimicrobial nanoparticles

Generally, antimicrobial NPs shows excellent antimicrobial activity because the high surface area to volume ratio of NPs gives good contact to cell. The working mechanisms of antimicrobial NPs have been frequently discussed in the literature on silver NPs. The proposed cytotoxicity mechanisms include: 1) disruption of bacterial cell membrane integrity,[21, 59, 60] 2) generation of reactive oxygen species,[61] 3) damage of bacterial protein and enzymes,[59, 62] 4) damage or inhibition of DNA replication,[62, 63] 5) disruption of cell respiration.[20, 59] Fig. 2-2 illustrates the different antimicrobial mechanisms on biofilm, intracellula, and cell membrane level. However, because some metal ions and metallic NPs, such as silver ions and silver NPs, both exhibit antimicrobial activity, the explanation of actual antimicrobial actions of these NPs remain ambiguous. For example, Mosselhy et al. compared the antimicrobial action between silver NPs and silver nitrate.[60] Results shows that there is a significant difference between the working mechanism of silver NPs and silver ions: silver NPs caused wall destruction, leakage cytoplasmic substances and gap between the cell wall and cell membranes, while silver ions tended to disrupt and damage bacterial DNA. Moreover, Dong et al. discovered that

the antimicrobial efficiency of silver NPs were significantly different in aerobic and anaerobic environment, which provides evidence of dynamic NPs-cell interaction that may undergo dissolution-reduction cycles in alternating environment.[64] In conclusion, the study on working aspects of antimicrobial NPs has not come to a certain conclusion, but the discovered cytotoxic mechanism can provide insights for developing new antimicrobial nanomaterials and potential clinical applications.

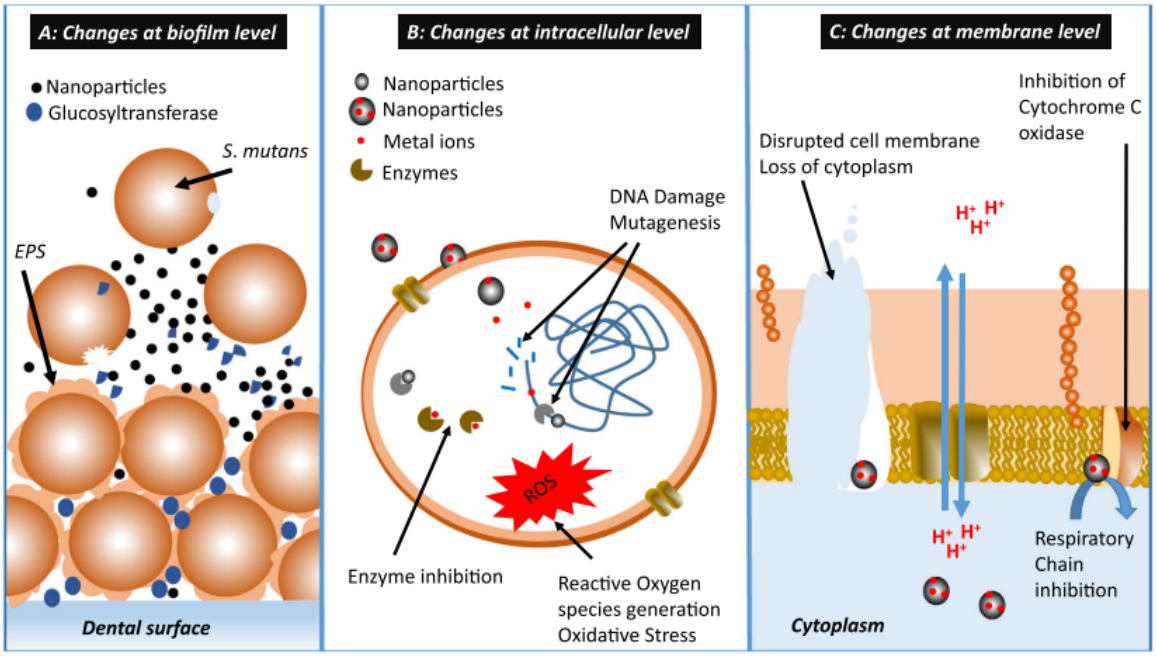

Figure 2-2 The functioning mechanism of antibacterial nanoparticles. (Adapted from Khan et al.[29])

2.2 Cellulose nanocrystals

2.2.1 Development of green nanotechnology and natural nanomaterials

With the rapidly growing market for nanotechnology and increasing applications of nanomaterials, concerns on nanomaterial-related safety and environmental issues has been raised. For example, Ag NPs is one of the most commonly identified

nanotechnology with over 500 commercial products that contain Ag NPs.[65] However, contrary to the considerable use of Ag NPs, few effective methods have been taken to recover these NPs. Donner et al. and Wang et al. show that these Ag NPs eventually enters soils through wastewater−sludge−soil pathway and are able to remain in their stable form for a period longer than 50 years, which can potentially harm microorganisms in soil and cause problems in algriculture.[66, 67] Although significant progress has been made to examine the toxicity mechanism of antimicrobial NPs, risks of long-term exposure to these nanomaterials remain unclear.[68-71] Considering the potential eco-toxicity, the incorporation of the fundamental principles of green chemistry and chemical process to nanotechnology has appealed to researchers and extended to a new market of sustainable green nanomaterials. As a result, nanotechnology and nanomaterials based on bio-resource has attracted increasing interest in recent years because they can be easily obtained and tend to bring less environmental impact.[72] Therefore, it is important for researchers to identify and utilize natural materials in nanotechnology.

As the most abundant natural material on earth, cellulose holds a key role. The global cellulose market is USD 219.53 billion in 2018 and is estimated to reach USD 305.08 billion by 2026, with a compound annual growth rate (CAGR) of 4.2%.[73] While cellulose has been used in paper and textile since the beginning of history, in the past two decades, growing research interest has been focusing on its applications in nanoscale due to the adequate quantity and versatility in terms of production of the nanomaterial.[74-79] Natural cellulose occurs in a hierarchical structure and semi-crystalline form (Fig. 2-3a), which allows the extraction of several different micro- or nano-cellulose materials, such as microcrystalline cellulose (MCC), cellulose nanofibers (CNF), and cellulose

nanocrystals (CNC). Each nanocellulosic material has its distinct properties and advantages which determine its applications.[79] Among them, CNCs, also referred to cellulose nano-whiskers or nanoparticles are obtained from the crystalline domain of cellulose and have been used as a special functional nanomaterial. The unique properties and applications of CNCs will be comprehensively discussed in the following sections. Fig. 2-3b shows the chemical structure of cellulose, which consists of long repeating anhydro-D-glucopyranose units (AGU) covalently linked through acetal functions between C_1 and C_4 atom. The unique β-1,4 glycosidic linkages between AGUs of cellulose construct an extensive linear-chain structure with considerable amount of hydroxyl groups and the chain-length is determined by the number of AGUs presented, i.e. degree of polymerization (DP), of cellulose. Typical DP of cellulose ranges from 300-20,000, depending on the raw material and extraction process.[76, 80, 81] Therefore, the extracting method plays a critical role in the physicochemical properties of nanocellulose.

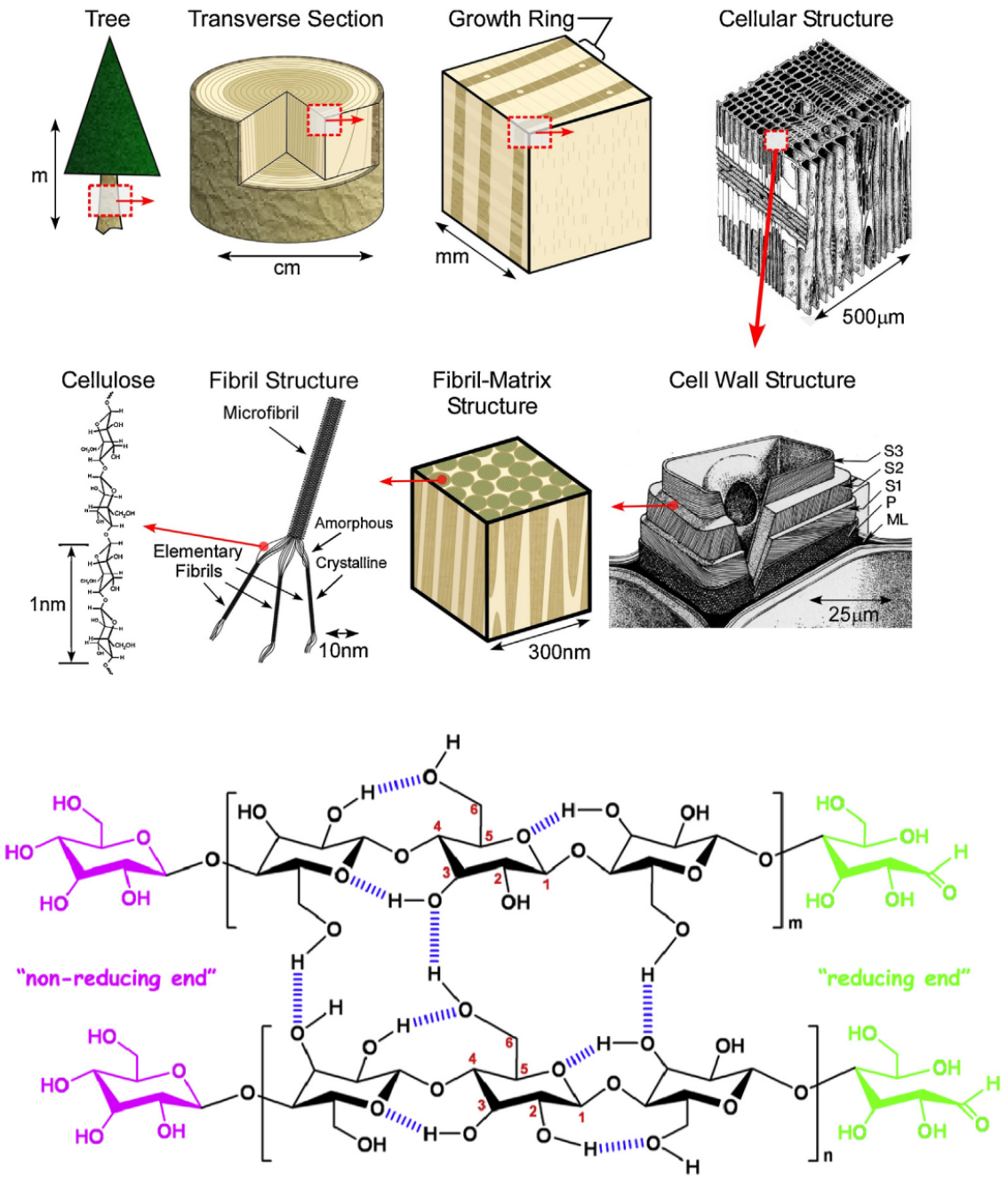

Figure 2-3 (a) A schematic illustration of the hierarchical structure of natural cellulose material from wood to cellulose. (adapted from Dufresne[76]) (b) Chemical structure and intra- and inter-molecular hydrogen bonding in crystalline cellulose. (adapted from Lin et al.[77])

2.2.2 Extraction and production of cellulose nanocrystals

Over the last two decades, significant progress has been made on the extraction technique of CNCs. Thus far, two companies have pushed the commercial production of CNCs to a large scale: CelluForce (Canada, 1000 kg day^{-1}), American Process (USA, 500 kg day^{-1}).[72] The successful commercial production of CNCs in return becomes more appealing for researchers to develop more advanced extracting methods aiming at lowering cost, increase high-yield, and lower environmental impact as frequently reported in the literature. It is well-known that CNCs possess various morphologies and physiochemical properties resulting from different extraction processes and sources.

Generally, CNCs extracted from natural sources are processed through a refined procedure to remove impurities in the fibril-matrix structure, such as lignin to produce cellulose fibers. The resulting cellulose fibers consist of highly ordered crystalline and amorphous domains, and the proportion of each fraction depends on the source.[82] These cellulose microfibrils undergo further extraction to isolate crystalline cellulose and finally form separate CNCs. Some of the reported extracting methods are listed in Table 1, which includes acid hydrolysis,[83-87] oxidation,[88, 89] and mechanical refinement.[90, 91]

Among them, acid hydrolysis is the most commonly used process where acid breaks the glycosidic bonds within the cellulose molecular chains in the amorphous domains along the cellulose fibrils.[86, 87] The selective cleavage of cellulosic chains is due to the kinetics difference of hydrolysis between the amorphous and crystalline domains.[92] Studies have reported on the hydrolysis of nanocellulose using various acids, such as hydrochloric acid, sulfuric acid, phosphoric acid and citric acid.[72, 84-86] Still, hydrochloric acid and sulfuric acid are the most frequently used acids in the extraction of CNCs in

laboratories and industry. The acid used during the hydrolysis process often affects the properties of extracted CNCs. For instance, CNCs obtained from hydrochloric acid hydrolysis show low surface charge and have poor dispersibility in water while CNCs extracted using sulfuric acid have greater surface charge owing to the sulfate groups that yield a stable suspension in aqueous solution.[87]

Although these two methods are simple and efficient, the large water consumption and acidic wastewater generation are major challenges. Therefore, possible solutions have been reported, such as optimizing the procedure to recycle waste chemicals, applying weak acids as a substitution, and developing cleaner methods, such as mechanical refinement.[72, 91] In conclusion, the extraction of CNCs consists of a series of procedure that removes the matrix materials and amorphous nanocellulose domains. The choice of extraction process are usually determined by the required properties in experiments and practical applications.

Table 1. Different extracting methods of CNCs.

Type of Method	Raw Material	Treatment Process	Post-treatment	Reference
Acid Hydrolysis	Microcrystalline cellulose	Dilution, cation exchange resin hydrolysis, ultrasonication	Filtration, rinsing, centrifugation	Tang et al.[83]
	Pineapple leaf	Grinding, H_2SO_4 64% at 45 °C hydrolysis, dilution	Centrifugation, dialysis, ultrasonication	Santos et al.[85]
	Whatman filter paper	4 N HCl solution at 100 °C for 120 min	Centrifugation, dialysis, ultrasonication	Camarero Espinosa et al.[84]
		H_3PO_4 85% at 60 °C hydrolysis, dilution	Centrifugation, dialysis, ultrasonication	
	Microcrystalline cellulose	Citric/hydrochloric acid hydrolysis	Washing, centrifugation, freeze drying	Yu et al.[86]
	Bacterial cellulose	H_2SO_4/HCl mixture at 45 °C, dilution	Centrifugation, dialysis, ultrasonication	Vasconcelos et al. [87]
Mechanical Refinement	Microcrystalline cellulose	Swilling in water, ultrasonication at power of 1500 W	Centrifugation, freeze drying	Li et al.[90]
	Microcrystalline cellulose	Soaking in distilled water, ultrasonication	Washing, drying	Li et al.[91]
Oxidation	Bleached sugarcane bagasse pulp	Suspended in water, treatment with TEMPO/NaBr/NaClO system	Washing, centrifugation, ultrasonication	Zhang et al.[88]
	Softwood bleached kraft pulp Microcrystalline cellulose	Sonication, treatment with TEMPO/NaBr/NaClO system	Washing, centrifugation, freeze drying	Zhou et al.[89]

2.2.3 Physical properties of cellulose nanocrystals

Generally, CNCs consist of rod-like cellulose nano-whiskers which are highly crystalline. The length (*L*), width (*D*), and aspect ratio (*L/D*) are three critical physical dimensions of CNCs and mainly determined by the raw cellulosic source and extraction technique. Table 2 shows some of the reported CNCs extracted from various cellulosic sources. The dimensions and morphologies of CNCs are usually characterized by microscopic techniques, such as transmission electron microscopy (TEM), scanning electron microscopy (SEM), or atomic force microscopy (AFM). Most plant-sourced CNCs have lengths ranging from 100-300 nm and widths between 5-20 nm,[93-98] while some bacterial CNCs have larger dimensions up to 1000 nm in length.[99, 100] (Fig. 2-4) It is suggested that the higher portion of crystalline region from bacterial cellulose makes it more resistant to acid hydrolysis and results in CNCs with larger size.[72, 101] The rod-like CNCs have high aspect ratio up to 100, which provides some unique features, such as low percolated threshold in polymer matrix.[102-104] Moreover, CNCs possess excellent mechanical strength, with a tensile strength of 7500 MPa and Young's modulus of 110-220 GPa.[101] Compared with other reinforcement materials, such as 302 stainless steel, CNCs displays significantly higher tensile strength, Young's modulus, and much lower density.[72, 105] (Table 2) Therefore, a number of research have been investigating the reinforcement using CNCs as a nanofiller.

Peresin et al. studied the nanofiber composite of CNC/polyvinyl alcohol (PVA) with CNCs loading ranging from 0% to 15%.[106] It was discovered that CNCs increased the overall crystallinity of CNC/PVA and enhanced the Young's Modulus of PVA by 4 times compared to pure PVA. Another work by Xu et al. examined the morphology,

crystallinity, and optimized concentration of CNCs in CNC/polyethylene oxide (PEO) composite film.[107] The results show that the large CNCs' aspect ratio and strong CNCs-matrix binding lead to a 600% increase in strain-at-break and toughness. Moreover, some studies also suggest that CNCs enhanced thermal stability, swelling properties, self-healing properties of composite polymer film.[108-112] All these reported applications have been focusing on utilizing the high aspect ratio and excellent mechanical strength of CNCs and developing mechanically enhanced CNC composite materials. Apart from this, the study on the surface chemistry of CNCs have become appealing for researchers to investigate the functionalized CNCs nanocomposite, and this will be discussed in the following sections.

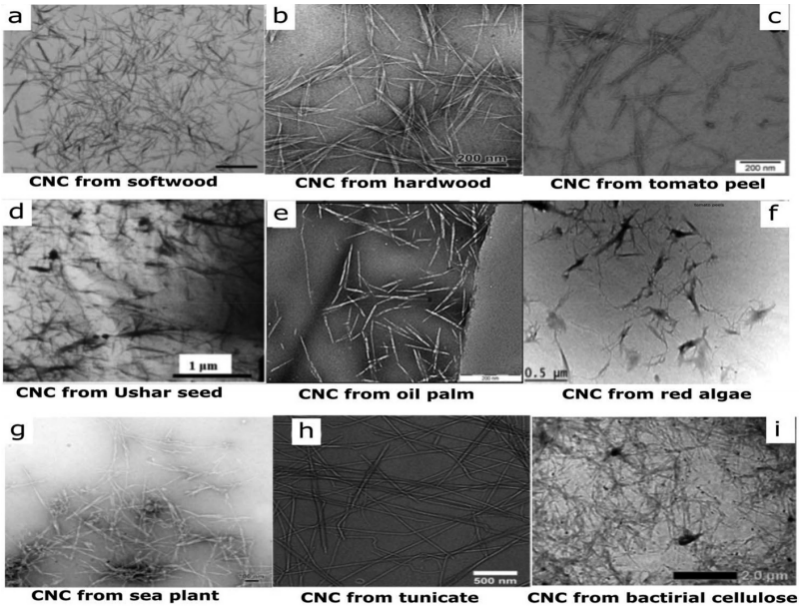

Figure 2-4 Morphologies of CNCs extracted from different bio-sources. (adapted from Trache et al.[72])

Table 2. Physical dimension of CNCs extracted from different sources.

Source	Extraction	Length (nm)	Width (nm)	Aspect ratio(L/D)	Reference
MCC	Acid hydrolysis	250-500	10-23	10-50	95, 96
Wood	Acid hydrolysis	100-300	3-5	20-100	81, 94, 98
Cotton	Acid hydrolysis	100-150	5-10	10-30	93
Ramie	Acid hydrolysis	70-200	5-15	5-40	97
Sisal	Acid hydrolysis	100-300	3-5	20-100	113
Bacteria	Acid hydrolysis	100-1000	10-50	2-100	99, 100

Table 3. Mechanical properties of some reinforcement materials.

Material	σ (MPa)	E (GPa)	ρ (g cm^{-3})	Reference
CNCs	7500-7700	110-220	1.6	Moon et al.[114]
Glass fiber	4800	86	2.5	Kim et al.[115]
302 stainless steel	1280	210	7.8	Hamad et al.[105]
Carbon fiber	4100	210	1.8	Moon et al.[114]

2.2.4 Surface chemistry and functionalization of CNCs

As mentioned in the previous sections, cellulose consists of repeating AGUs which are connected by β-1,4 glycosidic linkages. Each AGU possesses three hydroxyl groups (-OH), which provides CNCs with abundant surface functional groups that can be used in chemical modification. Apart from hydroxyl groups, CNCs may also have other functional groups owing to the extraction procedures. For example, CNCs extracted via sulfuric acid hydrolysis usually contain large amounts of sulfate ester groups ($-OSO_3^-$) which are negatively charged over a wide pH range and improve the dispersity of CNCs in aqueous solutions.[72] Also, CNCs extracted via citric acid hydrolysis or oxidation will have carboxyl groups ($-COO^-$) as surface anionic groups.[86, 89] Common surface functionalization methods, such as etherification, phosphorylation, silylation and amidation, utilize hydroxyl groups on CNCs to introduce new functional groups to the surface and enables a wide range of functions, such as stimuli-responsiveness and antimicrobial properties. Among these methods, polymer grafting is considered an attractive approach because the physical and chemical properties of grafted CNCs can be easily tailored without affecting the integrity of pristine CNCs, namely their dimensions, crystallinity, and mechanical strength.

Polymer grafting of CNCs can be performed using "grafting to" and "grafting from" methods. (Fig. 2-5a) "Grafting to" refers to attaching reactive end groups of pre-synthesized polymers to the surface of CNCs. However, the accessible hydroxyl groups on CNCs are limited and the long polymer chains often make it more difficult to graft high density of brushes onto the CNC surface due to steric hindrance.[101, 116] While "grafting to" method requires attaching the end groups of the polymer chains to the

surface of CNCs surface, on the other hand, "grafting from" method modifies the surface functional groups with small molecular initiator, and follows by the polymerization directly from the CNC surface. With less steric hindrance, "grafting from" methods can graft more initiators and hence the grafting density of polymers can be enhanced. Also, the polymerization from CNC surface prevents the possibility of physical coating of polymer chains to the surface CNCs, which is more favorable for quality control of the product.

Surface-initiated free radical polymerization (SI-FRP) is one of the most commonly used approaches to graft polymers from the CNC surface. The initiator is used to abstract hydrogen from the hydroxyl groups on CNCs generating reactive radicals on the CNC surface, where monomers react with the propagating chains. SI-FRP is a convenient and straight-forward approach to graft polymers with high molecular weight on CNCs. For example, Wu et al. used potassium persulfate (KPS) as a thermal initiator to perform SI-FRP on CNCs.[117] At temperature between 60-70 °C, hydrogen atoms were removed from the hydroxyl groups on CNC surface by the sulfate radicals generated by KPS. Poly-acrylic acid (PAA), a polymer with unique swelling properties, was successfully grafted onto the CNC surface. The resulting PAA-g-CNC was then incorporated within the CNC-based hydrogel that exhibited excellent water retention properties with a swelling ratio of 323 g/g in distilled water, which can be used as a sensitive material in water detection. Similarly, ammonium persulfate (APS) was used as a thermal initiator of SI-FRP to graft poly[2-(dimethylamino)ethyl methacrylate] (PDMAEMA) to CNCs.[118] The synthesized PDMAEMA-g-CNC had a tertiary amide loading of ~0.8 mmol/g CNCs and was used as a pH-responsive emulsifier in heptane-in-

water and toluene-in-water Pickering emulsions. Despite the simple process and high-molecular weight of grafted polymers, SI-FRP cannot control the grafting density, molecular weight, and composition of grafted polymers. Moreover, the introduction of thermal initiator, such as APS inevitably brings free polymers in bulk solution which may cause contamination issues in practical applications.

In order to graft polymers with controlled grafting density, molecular weight and architecture, surface-initiated controlled radical polymerization (SI-CRP) is used. In general, CRP is a living chain polymerization, where the reactions depend on the reversible deactivation of propagating chains with a first order kinetics. Polymers synthesized by CRP typically exhibit low polydispersity due to the negligible termination reactions.[119] In the synthesis of polymer grafted CNCs, copper-mediated surface-initiated atom transfer radical polymerization (SI-ATRP) is the most frequently used technique. Performing SI-ATRP from CNCs surface requires pre-treatment of pristine CNCs to introduce and immobilize the initiators onto the CNC surface. This is usually achieved by treating CNCs with α-bromoisobutyryl bromide (BiBB) in dimethylformamide (DMF) or tetrahydrofuran (THF).[120-124] A base (triethylamine) and a catalyst (4-dimethylaminopyridine) are often used to obtain a higher yield, and the grafting density of initiator can be controlled by adjusting the amounts of BiBB used during the reaction.[125, 126] With the presence of Cu(I) metal complex, the reverse deactivation of ATRP occurs through the exchange of bromine atoms between metal complex and propagating species. (Fig. 2-5b) The Cu mediated SI-ATRP is versatile and has been used to graft various of polymeric chains, such as polystyrene (PS),[122, 127, 128] poly(alkyl methacrylate),[129-131] PDMAEMA[132, 133] poly(N-isopropylacrylamide) (PNIPAM),[134, 135]

and poly(4-vinylpyridine) (P4VP).[136-138] Apart from homopolymers, SI-ATRP can also be used to graft copolymers due to its high tolerance to various functional groups.[120, 124, 133] However, ATRP is extremely sensitive to oxygen and requires a large quantity of transition metal complex as catalyst.[119, 137] These metal catalysts, such as Cu, are generally toxic and the removal of residual metal is difficult and not cost-efficient.

In order to overcome the oxygen sensitivity and minimize the metal catalyst, Activator Re-Generated by Electron Transfer (ARGET) ATRP was developed based on the principles of conventional ATRP. It was used by Hansson et al. to graft PMMA onto several types of cellulose substrates.[139] In the process, excess ascorbic acid was used as a reducing agent to continuously regenerate the Cu(I) species from Cu(II) species which were produced by radical termination in ATRP. The Cu(II) required in the process was reduced to 31.2 μmol and the surface grafting of PMMA was successfully performed. It is suggested that ARGET ATRP can reduce the required concentration of transition metal catalysts to the ppm level and is more tolerant to oxygen. Because of these advantages, researchers have conducted studies on CNC polymer grafting using this method. For example, Zhang et al. performed grafting of PS and P4VP from CNCs using both ATRP and ARGET ATRP.[137] The concentrations of Cu catalyst used in ATRP and ARGET ATRP were 2000 ppm and 20 ppm, respectively. In addition, a sacrificial initiator ethyl α-bromoisobutyrate (EBiB) was added to evaluate the molecular weight of grafted PMMA and P4VP polymers. It was found that despite the successful grafting of polymers using these methods, ARGET ATRP tend to grow longer polymer chains with lower grafting density on CNCs surface comparing with conventional ATRP. It is considered

that the much lower catalyst concentration and faster propagating rate of ARGET ATRP contributed to the different characteristics of grafted polymers.[137]

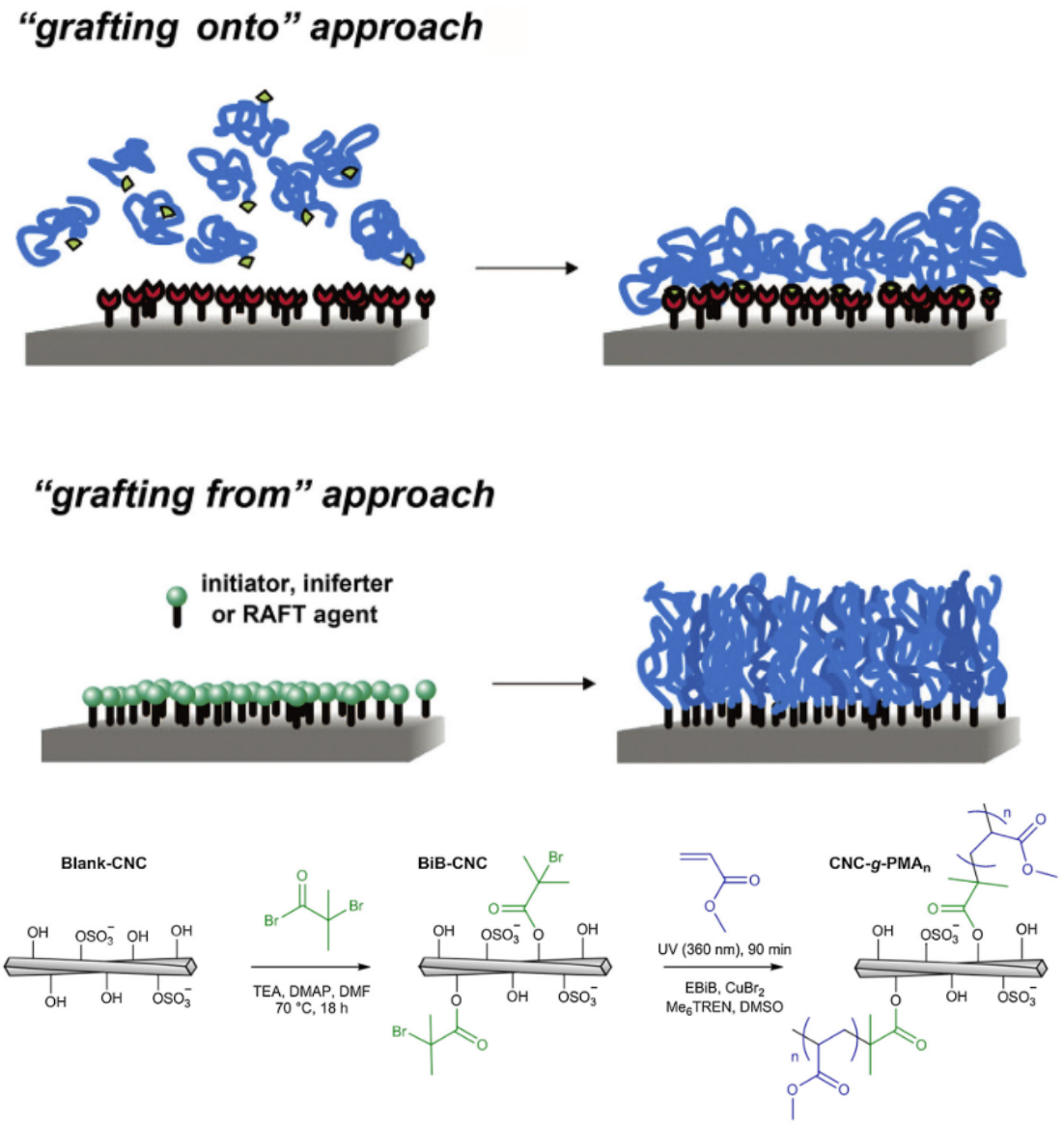

Figure 2-5 (a) A schematic illustration of "grafting to" and "grafting from" techniques. (adapted from Zhao et al.[140]) (b) Grafting PMMA from CNCs surface using SI-ATRP (adapted from Hatton et al.[130])

2.2.5 Cellulose nanocrystals for antimicrobial applications

It has been discussed in the previous sections that various nanomaterials, such as Ag NPs possess strong antimicrobial activities. Despite their excellent antimicrobial activity of existing metallic NPs or metal/polymer nanocomposites, the potential eco-toxicity has limited the applications of these antimicrobial nanomaterials.[71, 141, 142] Therefore, research has focused on green chemical process to synthesize effective antimicrobial nanomaterials. CNC is a bio-sourced nanomaterial with good biocompatibility, biodegradability, high mechanical strength, high aspect ratio and excellent colloidal stability, which can be considered as a great candidate of a green antimicrobial nanomaterial. However, most CNCs are extracted from acid hydrolysis and have abundant negatively charged surface functional groups, such as sulfate ester group ($-OSO_3^-$), which generate electrostatic repulsion between CNCs and bacteria cell wall. Therefore, many studies have demonstrated various surface modification of CNCs to increase stability and antimicrobial effects.

One major approach to prepare antimicrobial CNCs is the incorporation of existing antimicrobial NPs.[143-148] For example, Wang et al. reported a green synthesis of CNC/AgNPs nanocomposite using CNCs as bio-substrate and glucose as reducing agent for Ag NPs at room temperature.[149] The negatively charged sulfate groups on CNCs can adsorb Ag^+ in solution and thus facilitate the nucleation of Ag NPs. The antibacterial tests against *E. coli* and *S. aureus* shows that synthesized CNC/AgNPs exhibit stronger antibacterial activity than commercial Ag NPs by 50% lower MIC. It is suggested the better dispersity and colloidal stability of CNC/AgNPs lead to the higher antibacterial

efficiency. In general, this approach utilized the negatively charged CNCs as substrate to stabilize and disperse antimicrobial NPs. Another similar approach is the coating of metal onto CNC surface to form a core-shell structure of metal nanorods or nanoclusters.[150, 151] Apart from loading metallic NPs to achieve antimicrobial activity, CNCs can also be used to graft or carry antimicrobial materials due to versatile functionalization and amphiphilic nature of cellulose. Castro et al. prepared antimicrobial rosin grafted CNCs by a one-pot green synthetic process.[152] Rosin is a natural product of pine resin that consists of several different hydrophenanthrene structures and shows antimicrobial activity. Rosin was successfully grafted through esterification and showed strong antibacterial activity against gram-negative bacteria. In another study, Tang et al. synthesized polyrhodanine-coated (PR) CNCs by in-situ polymerization in aqueous solution.[153] The prepared PR-CNCs showed promising antimicrobial properties toward both *E. coli* and *B. subtilis* and low cytotoxicity. The use of CNCs substrate enables the dispersion of PR in aqueous solution and thus enhance its antimicrobial activity.

Apart from using CNCs as a substrate or carrier for antimicrobial NPs and drugs, there is a growing interest for researchers to develop cationic CNCs as antimicrobial agents. Since both Gram-positive and Gram-negative bacterial have negatively charged cell wall, cationic CNCs can directly interact with bacteria and disrupt cell membrane and cause the leakage of cytoplasmic contents.[154] While various methods has been reported to synthesize cationic CNCs derivatives, the introduction of quaternary ammonium functional groups is one of the most frequently reported approach.[154-160] (Table 4) Quaternary ammonium compounds (QACs) are positively charged and have high antimicrobial activity by interacting with membrane structure of microbes. The types,

efficiency, and working mechanism of QACs will be discussed in the following sections. Bespalova et al. reported a two-step synthesis of antimicrobial quaternary ammonium CNCs (Q-CNCs).[157] The modification of CNCs was performed by chloroacetylation and subsequent reaction with tertiary amines with different alkyl chain lengths. Q-CNCs were successfully synthesized and the results showed that Q-CNCs with long alkyl chains longer than 10 carbons exhibited strong antimicrobial activities. Another study conducted by Liu et al. used epoxypropyltrimethylammonium chloride (EPTMAC) and other two similar QACs to prepare Q-CNCs through a one-step nucleophilic addition reaction.[158] The grafted CNCs was used as a filler in chitosan films to enhance the mechanical properties and antimicrobial activity.

Table 4. Summary of QACs modified cellulose materials. (adapted from Tavakolian et al.[154])

QAC type	Cellulosic material	Antibacterial activity
Cetyltrimethylammonium bromide	Sulfate-modified CNCs	NA
	hyperbranched polyethylene ionomers-modified CNCs	
3-chloro-2-hydroxypropyl-trimethyl ammonium chloride	Cellulosic triacetate reverse osmosis membranes	*E. coli* and *S. aureus*
3-(trimethoxysilyl)-propyldimethyloctadecyl ammonium chloride	Cellulose fibers	*E. coli* and *S. aureus*
Quaternized 2-(dimethylamino) ethyl methacrylate	TEMPO-mediated CNC	*E. coli* and *S. aureus*
2,3-epoxypropyl trimethylammonium chloride	Enzymatic microfibrillated cellulose	*B. subtilis* and *S. aureus*
	CNFs	NA
Trimethoxysilylpropyl octadecyldimethyl ammonium chloride	Cellulose fibers	*B. cereus, E. coli, P. aeruginosa*
(3-Carboxypropyl) trimethylammonium chloride	Cellulose-based photosensitizer	*E. coli* and *S. aureus*
Girard's reagent T	Foams made of CNFs	*E. coli*
Dilinoleic acid-athylenediamine compound	Bacterial cellulose membrane	*S. aureus* and *S. epidermidis*
N-(2-ethoxy-2-oxoethyl)-*N*,*N*-dimethylprop-2yn-1-aminium bromide	Azide-modified cellulose	*E. coli*
Hexadecyltrimethylammonium bromide	Sulfate-modified CNC	NA
Poly(isopropanol dimethylammonium) chloride	Filter paper	*E. coli*
N-[(2-hydroxy-3-trimethylammonium) propyl] chitosan chloride	Cellulose acetate electrospun nanofibrous mats	*E. coli* and *S. aureus*

2.3 Quaternary ammonium compounds and polymeric antimicrobial materials

2.3.1 Introduction to quaternary ammonium compounds

Quaternary ammonium compounds (QACs) refers to compounds that have an amine group covalently bonded to four residues, making the quaternary ammonium group positively charged and it is usually accompanied with a halide anion. For common linear alkylammonium QACs (Fig. 2-6a), one (or two) of the four residues connected to the cationic headgroups is usually a hydrophobic long alky chain while other groups are often short-chain substituents such as methyl or benzyl groups. Due to the amphiphilic chemical structure of QACs, they are also referred to as quaternary ammonium surfactants and offer a good utility in a variety of applications, such as disinfectants, fabric softeners, detergents, and personal care products.[161-163]

The positively charged head group and amphiphilic property makes QACs potential antimicrobial agents because bacterial cell walls are negatively charged, and the cell membrane can be disrupted through a "detergent-like" mechanism. As shown in Fig. 2-6b, QACs are electrostatically attracted to the bacterial cell and the alkyl chains subsequently bind to the cell membrane. The disruption and thinning of the bacterial membrane lead to leakage of cytoplasmic materials, autolysis, and cell death.[162, 164, 165] Since the working mechanism strongly depends on the hydrophobic alkyl chain on the amine groups, studies have been conducted to investigate the relationship between the alkyl chain length and the antimicrobial activity of QACs. Li et al. synthesized QACs - from 2-(dimethylamino) ethyl methacrylate (DMAEMA) and organo-halides with alkyl chain length ranging from 3 carbons to 18 carbons using the Menschutkin reaction .[166] The results showed that the antimicrobial activity increased dramatically (5 times lower

MIC) when the increasing alkyl chain length was increased from 3 to 15. However, QACs with 18-carbon alkyl chain showed a reduction in antimicrobial activity. Other similar research conducted by Zhou et al.,[167, 168] Liang et al.,[168] and have shown results that were consistent with previous experiments that linear QACs with a alkyl chain length at 15 carbons shows the highest antimicrobial activity. Moreover, Xu et al. studied the antimicrobial activity of QACs with the same alkyl chain length but different short-chain quaternary ammonium group substituents.[169] It is suggested that the benzyl substituent showed lower MIC than methyl groups against *S. mutans* and inhibition of biofilm, which can be potentially used in applications, such as dental materials.

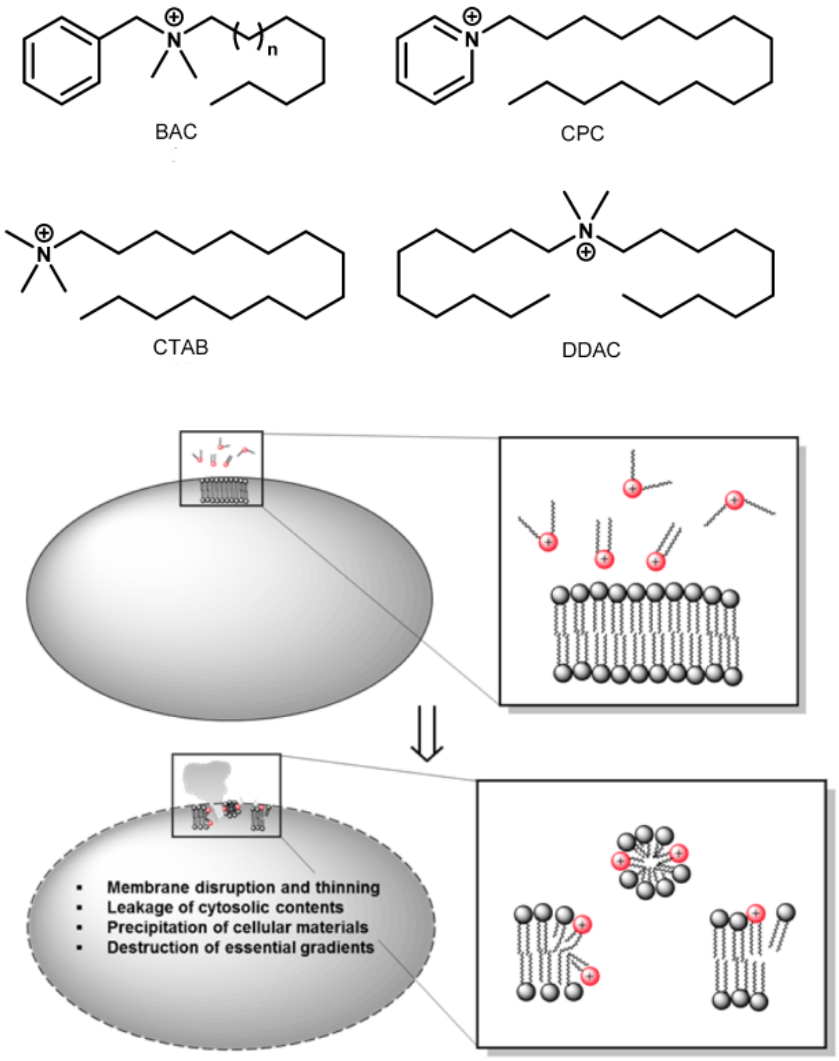

Figure 2-6 (a) Structure of some common commercial QACs (b) Antimicrobial mechanism of QACs. (adapted from Jennings et al.[162])

2.3.2 Polymer with quaternary ammonium groups

Antimicrobial resistance has been a great challenge for all antimicrobial materials. It is well-known that bacteria gain resistance under long-term exposure to antibiotics and the development of antibiotic-resistant microorganisms has been identified by WHO as a global critical health challenge.[170, 171] QACs were once not considered an issue in terms of resistance because the working mechanism of QACs is by contacting and physically disrupting the cell membrane.[165, 172, 173] However, in the last two decades, researchers have discovered the possible relationship between drug resistance and the clinical use of QACs, as well as the antimicrobial resistance to QACs.[174-176] QACs are widely used as disinfectants and surfactants which will be released to environment together with the wastewater. The presence of QACs at sub-inhibitory concentrations in the environment become selective and favorable to the survival of microorganism with lower susceptibility, which will eventually result in the development of QAC-resistant microbes.[163, 172, 176] Therefore, it is important to develop alternative antimicrobial methods to prevent QACs from being released to the environment. Compared with the commonly used monomeric QACs, polymeric QAC structures are capable of overcoming some of the limitations.[177-179] Moreover, it was also reported that polymerized QACs enhanced the antimicrobial activity under certain conditions.[167]

Chapter 3 Surface modification of CNCs by ARGET-ATRP and quaternization

3.1 Introduction

Over the last two decades, there has been a tremendous growth in the application of nanotechnology and nanomaterials in biomedical applications. Among them, the antimicrobial properties of nanomaterials have been frequently studied. Due to the small dimensions, nanoparticles can easily interact and enter the cell structure of microorganisms and inhibit vital cytoplasmic activities, such as respiration and DNA replication.[19, 21, 25, 180] Moreover, the high surface-to-volume ratio and electric charge on NPs contribute to the disruption of bacterial cell membrane and further enhance the antimicrobial activities.[21, 59, 60]

Cellulose nanocrystals (CNCs) are crystalline cellulose nano-rods extracted from natural cellulosic fibrils via acid hydrolysis. As bio-sourced NPs, CNCs have been frequently used in biomedical research and applications due to its favourable properties, such as robust mechanical strength, high aspect ratio, biocompatibility, biodegradability, and colloidal stability.[101, 181] Although the negatively charged pristine CNCs surface sulfate groups resulted from sulfuric acid hydrolysis greatly limit their effective electrostatic interactions with bacteria and fungi, the versatile surface functionalization and amphiphilic nature of CNCs have provided researchers with various approaches to develop antimicrobial NPs.[149-151, 158] For example, the intrinsic negative charge on CNCs and the excellent colloidal stability makes it ideal templates for the nucleation and stabilization of metallic nanoparticles. Therefore, studies have been focused on decorating the CNCs with inorganic antimicrobial NPs such as Ag NPs, gold NPs, and ZnO NPs.[144, 146, 149, 150, 182, 183] The use of CNCs not only prevents the use of toxic

chemicals, such as $NaBH_4$ but also enhance the stability of the bound NPs in aqueous solution. Also, other studies have utilized CNCs to carry antimicrobial drugs as another approach to achieve antimicrobial activity.[152, 153, 184]

Recently, there have been more research on preparing antimicrobial CNCs by altering their surface charge. It is well known that quaternary ammonium compounds (QACs) have strong antimicrobial activity due to the high affinity of the negatively charged phospholipids bacteria cell membrane to the positively charged nitrogen headgroup. Efforts have been made to covalently graft QACs onto various cellulosic surface groups, for example, chloroacetylation and quaternization of hydroxyl groups,[157] or one-step reaction using epoxy or silane QA salts.[154, 158, 185] However, most of these studies focused on application of surface modification of bulk cellulose in textile, or using the antimicrobial CNCs as a filler for polymer matrix and films.[155, 157, 158, 160] Few researchers have examined the QAC-based cationic CNCs as antimicrobial nanomaterials in colloidal system. One of the major challenges is that the stability of pristine CNCs rely on the strong negative charge on the surface, the surface grafted cationic quaternary ammonium groups must be sufficient to make strong positive net charge and maintain the colloidal stability. Also, the density of quaternary groups on CNCs should be high enough to achieve antimicrobial activity.

In this study, we develop a cationic polymer-grafted antimicrobial CNC system via CNC-surface initiated ARGET-ATRP. The quaternary ammonium groups on the polymer side chains will provide the CNC surface with a large amount of positive charge yielding cationic CNCs. The design of this CNC-based cationic polymer "brush" by SI-ATRP makes it possible to completely recover the polymer after treatment and reduced

the potential environmental impact of antimicrobial polymer residue. Also, the high local concentration of quaternary ammonium groups on polymer grafted CNCs can potentially enhanced the antimicrobial activity.

3.2 Experimental procedure

3.2.1 Materials

Cellulose Nanocrystals were supplied by Celluforce (Montreal, Quebec). α-Bromoisobutyryl bromide (BIBB), 4-(dimethylamino)pyridine (DMAP), triethylamine (TEA), N,N-dimethylformamide (DMF, anhydrous, 99.8%), 2-(dimethylamino)ethyl methacrylate (DMAEMA), copper(II) bromide ($CuBr_2$), N,N,N′,N′′,N′′-pentamethyldiethylenetriamine (PMDETA), L-Ascorbic acid, benzyl bromide, (2-bromoethyl) benzene, 1-bromo-3-phenylpropane were purchased from Sigma Aldrich (St. Louis, USA). Dimethyl sulfoxide (DMSO) were purchased from Fisher Scientific. All chemicals were used without further purification. Milli-Q water was used in the preparation of aqueous dispersion.

3.2.2 Immobilization of BIBB initiator on CNCs

1 g CNCs were dried and dispersed in 100 mL DMF by ultrasonication for 30 mins. The suspension was transferred to a 250 mL round flask and 4 mL TEA, 3.00 g DMAP were added. The mixture was then placed in an ice-bath and stirred at 400 rpm under nitrogen for 30 min. Then, BIBB (6 mL) was dropwise added to the reaction mixture. After 24 h, the product was thoroughly washed with ethanol, and dialyzed with water for 3 days. The resulted CNC-Br was freeze dried and stored in the fridge.

3.2.3 ARGET-ATRP of DMAEMA using CNC-Br initiator

400 mg CNC-Br was dispersed in 40 mL DMF via ultrasonication for 30 min. The suspension was transferred to a 100 mL round flask and 6 mg $CuBr_2$, 24 μL PMDETA and 2.02 mL (12 mmol) DMAEMA were added. The mixture was then pumpedbubbled with dry nitrogen for 1 h to completely remove the remaining oxygen in

the system. The suspension was then heated and kept at 60 °C with 400 rpm stirring. The polymerization was initiated by dropwise addition of 5 mL (10 mg/mL in DMF) ascorbic acid and the reaction was kept stirring for 24 h at 60°C. After polymerization, the obtained PDMAEMA-g-CNC was thoroughly washed with THF, ethanol, and water, and then dialyzed against water for 3 days. The synthesized sample was stored in water suspension and part of the sample was freeze-dried for quaternization.

3.2.4 Quaternization of PDMAEMA-g-CNCs

50 mg PDMAEMA-g-CNCs was dispersed in 9 mL DMSO by ultrasonication and transferred to a 20 mL flask. 1 mL of quaternizating agent (benzyl bromide, (2-bromoethyl) benzene, 1-chloro-3-phenylpropane) was then added and the reaction was kept at room temperature for 24 h. The synthesized Q-CNC was then washed with acetone, ethanol, water and then dialyzed with water for 3 days. The obtained samples were kept in water suspension.

3.2.5 Physical and chemical characterization

The morphologies of the samples were examined using a Philips CM10 transmission electron microscope at an accelerating voltage of 60 kV. The transmission electron microscopy (TEM) samples were prepared by depositing a droplet of each sample (0.01 wt %, sonicated in an ice bath) on a copper grid, and the excess water was removed via evaporation at room temperature. Fourier transform infrared (FTIR) spectrometry was conducted using a PerkinElmer Spectrum Two over the range of 400−4000 cm^{-1} by taking an average of 16 scans (resolution of 4 cm^{-1}).

3.2.6 Particle size and zeta potential measurement

The average particle size and zeta potential measurements were conducted using Zeta-potential analyzer (Nanosizer ZS, Malvern, UK) by taking an average of 3 measurements of 10-120 scans to minimize inaccuracy. The synthesized CNC samples were diluted to 0.02% and ultrasonicated for 10 min before each analysis.

3.2.7 Titration of PDMAEMA-g-CNC and Q-CNCs

PDMAEMA-g-CNC (20 mL of 0.0125%) suspension was adjust to pH 3.6 and then titrated with 0.01 M NaOH to determine the amounts of tertiary ammonium groups. Q-CNC-1 (20 mL of 0.025%) and Q-CNC-2 (20 mL of 0.025%) suspension was titrated by 10 mM $AgNO_3$ to determine the quantity of quaternary ammonium groups. The conductivity was measured and plotted with titrant volume to obtain the titration curve. The tertiary ammonium groups (N_{TA}, in mmol/g) can be calculated using the following equation:

$$N_{TA} = \frac{(V_2 - V_1) \times C_{NaOH}}{m_{sample}} \quad (1)$$

where V_1 is the starting point of deprotonation (mL), V_2 is the end point of deprotonation (mL), C_{NaOH} is the concentration of NaOH titrant used (mmol/L), and m_{sample} is the mass of PDMAEMA-g-CNC titrated (g). Similarly, the quaternary ammonium groups (N_{TA}, in mmol/g) can be calculated using the following equation:

$$N_{QA} = \frac{V_t \times C_{AgNO_3}}{m_{sample}} \quad (2)$$

where V_t is the end point of precipitation where the conductivity starts to increase (mL), C_{AgNO3} is the concentration of $AgNO_3$ titrant used (mmol/L), and m_{sample} is the mass of Q-CNC titrated (g).

The degree of quaternization (*DQ*) can be estimated using the following equation:

$$DQ = \frac{N_{QA}}{N_{TA}} \quad (3)$$

where N_{QA} and N_{TA} are the molar amount of quaternary ammonium groups per gram and the molar amount of quaternary ammonium groups per gram, respectively.

3.2.8 Antimicrobial tests using *Saccharomyces cerevisiae* (yeast)

The antimicrobial activity of quaternized PDMAEMA-g-CNC was evaluated using yeast as a model microorganism. The carbon dioxide (CO_2) production of the yeast in a 30-min period was measured every 30 seconds to quantitatively compare the inhibitory effect of PDMAEMA-g-CNC with different degree of quaternization. The experimental setup is shown in Fig. 3-1. 50 mg yeast and 50 mg D-(+)-glucose were dissolved and mixed in 5 mL Milli-Q water (pH 6.0) in a 10 mL flask. After adding CNCs samples, the mixture was placed in a water bath at 42 °C and stirred at 300 rpm. The flask was then sealed, and the generated CO_2 was collected and measured using a burette filled with water.

Figure 3-1 A photograph of the experimental setup for antimicrobial test.

3.3 Results and discussion

3.3.1 Synthesis of PDMAEMA-g-CNC and quaternization of PDMAEMA-g-CNC

PDMAEMA-g-CNC was synthesized by ARGET-ATRP using CNC-based macro-initiator in Cu/PMDETA catalytic system. The general process is shown in Fig. 3-2a. To begin with, CNC-Br macro-initiator was prepared by esterification of surface hydroxyl groups using BIBB. The obtained CNC-Br was then used as initiator for ARGET-ATRP of DMAEMA. In the process, excess ascorbic acid was used as a reducing agent to continuously regenerate the Cu(I) species from Cu(II) species, which

were produced by radical termination in ATRP, which minimized the use of Cu ions and greatly enhanced the oxygen tolerance of ATRP.

The following quaternization of PDMAEMA-g-CNCs was carried by Menschutkin reaction using three different quaternizing agents, namely, benzyl bromide, (2-bromoethyl) benzene, 1-bromo-3-phenylpropane. The obtained quaternized PDMAEMA-g-CNC were noted as Q-CNC-1, Q-CNC-2, and Q-CNC-3, respectively. The synthesis of Q-CNC-1 is shown in Fig.3-2b as an example. The benzyl bromide reacted with a tertiary ammonium group on the PDMAEMA and converted it to a quaternary ammonium group with a bromine counter ion. The synthesis of Q-CNC-2 and Q-CNC-3 follows the same principle. Three different quaternizing agents were used to compare the difference in quaternization and the potential different antimicrobial activity of the three different Q-CNC samples.

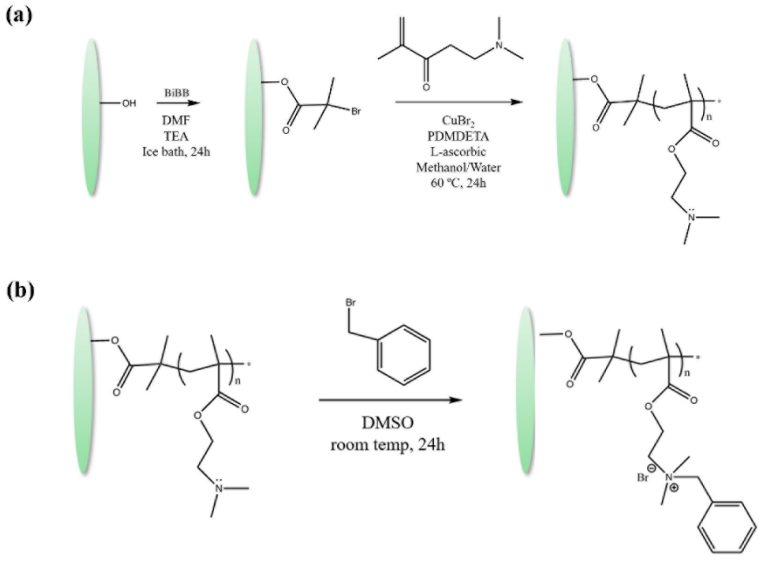

Figure 3-2 A schematic illustration of (a) CNCs surface-initiated ARGET-ATRP, (b) synthesis of Q-CNC-1.

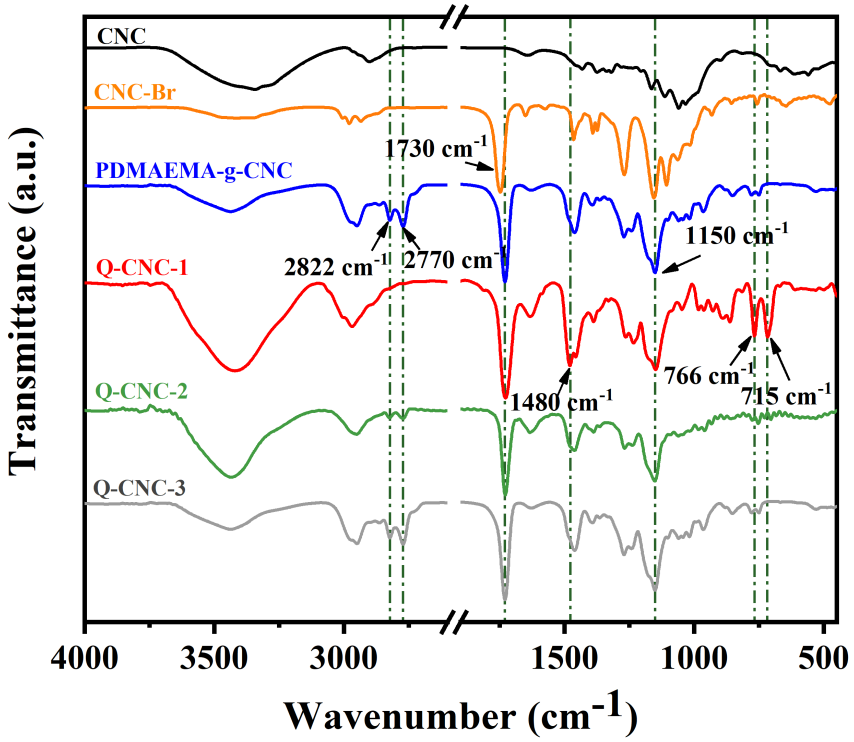

Figure 3-3 FTIR results of CNC (black), CNC-Br (orange), PDMAEMA-g-CNC (blue), Q-CNC-1 (red), Q-CNC-2 (green), Q-CNC-3 (grey).

The FTIR results of CNC, CNC-Br, PDMAEMA-g-CNC, Q-CNC-1, Q-CNC-2, and Q-CNC-3 are shown in Fig.3-3. After the esterification of pristine CNCs, a new peak at 1730 cm^{-1} was observed, which was attributed to the C=O stretching on CNC-Br, indicating the successful immobilization of BIBB initiators on CNCs. PDMAEMA-g-CNC shows stronger peaks at 1730 cm^{-1} because of the additional carbonyl groups on PDMAEMA side chains. Also, the peak observed at 1150 cm^{-1} correspond to the C-N stretching on the tertiary ammonium groups.[159, 186] Other peaks at 2822 cm^{-1} and 2770 cm^{-1} are attributed to the out-of-plane C-H bending of PDMAEMA.[159, 187] The peaks observed from PDMAEMA-g-CNC suggests the successful grafting of PDMAEMA onto

CNCs surface. After quaternization with benzyl bromide, the obtained Q-CNC-1 shows strong peaks at 766 cm^{-1}, 715 cm^{-1}, and 1480 cm^{-1}, which indicates the substituted benzyl groups on quaternary ammonium groups. Due to the difference in degree of quaternization (which will be discussed in the following sections), the same peaks were observed at a lower intensity in Q-CNC-2 and can hardly be observed in Q-CNC-3.

3.3.2 Morphology of CNCs, CNC-Br, PDMAEMA-g-CNC, and Q-CNC

The TEM image of CNCs, CNC-Br, PDMAEMA-g-CNC, and Q-CNC-1-3 are shown in Fig. 3-4. As shown in Fig. 3-4a, CNCs have negative surface charge and could form a stable colloidal suspension in water. As a result, individual CNCs had clear edges and the average length of CNCs were around 300 nm. The esterification with BIBB increased the hydrophobicity of CNCs, which could lead to the slight aggregation of CNC-Br and the edge became vague due to the initiators grafted on CNCs. (Fig. 3-4b) After polymerization, the particle size of PDMAEMA-g-CNC dramatically increased to over 500 nm due to two reasons: 1) the heavily grafted long-chain PDMAEMA increased the size of CNC brush, and 2) the partially positively charged PDMAEMA-g-CNCs crosslinked with other CNCs and formed a physical cross-linked nanogel. (Fig, 3-4c) While the Q-CNC-1 and Q-CNC-2 shows almost identical morphology with dimensions of between 300-500 nm, Q-CNC-3 shows similar structure to non-quaternized PDMAEMA-g-CNCs, which will be discussed in the later sections. (Fig. 3-4def) In conclusion, the ATRP grafting of PDMAEMA increased the size of CNCs and the quaternization could reduce the aggregation and stabilized the Q-CNC particles.

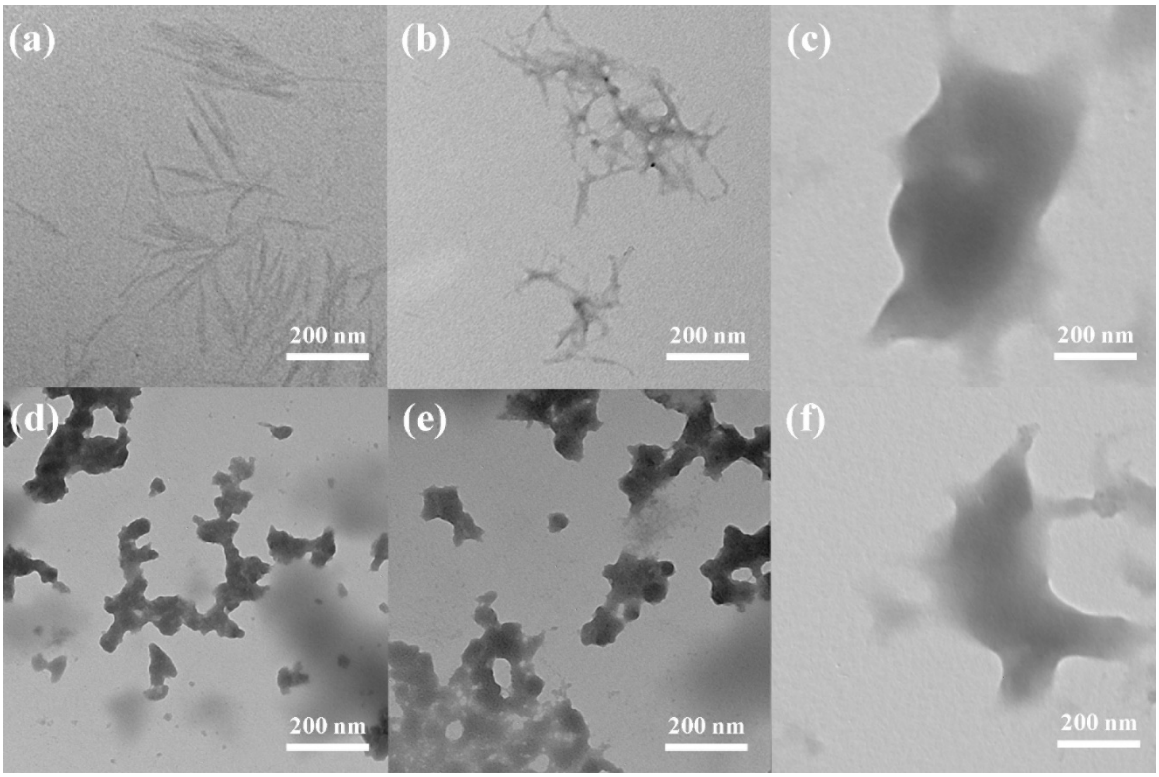

Figure 3-4 TEM images of (a) CNCs, (b) CNC-Br, (c) PDMAEMA-g-CNC, (d) Q-CNC-1, (e) Q-CNC-2, and (f) Q-CNC-3.

3.3.3 Surface charge and colloidal stability of PDMAEMA-g-CNC and Q-CNC

CNCs extracted via sulfuric acid hydrolysis have excellent colloidal stability because of the large amounts of negatively charged sulfate ester groups that retain their charge over a wide pH range. The zeta potential of CNCs used in this study were determined to be -45 mV. PDMAEMA is known as a pH-responsive polymer because of the tertiary ammonium groups on its side chains with a pK_a of around 7.4 at room temperature.[188, 189] The zeta potential and particle size of PDMAEMA-g-CNC is shown in Fig. 3-5a. At pH ranging from 4 to 7, PDMAEMA-g-CNC exhibited zeta potential at around +20 mV, which can be explained by the protonation of tertiary ammonium groups

on the PDMAEMA side chains with the presence of high proton concentration. (Fig. 3-6) The particle size increased from 550 nm to over 600 nm with the increasing pH from 4-7, which is due the partial deprotonation of amine groups inducing the aggregation of PDMAEMA-g-CNC. With the further increase in the pH, the size of PDMAEMA-g-CNC decreased due to the shrinkage of the grafted PDMAEMA polymer chains due to increasing hydrophobicity after deprotonation. The inset of Fig. 3-5a showed the stability of PDMAEMA-g-CNC after 30 min at different pHs. The sample at pH 4 exhibited good dispersity, while the rest of samples quickly precipitated in aqueous solution. This can also be explained by the densely grafted PDMAEMA which increased the hydrophobicity of CNCs, which will be further investigated in the following sections.

After the quaternization using benzyl bromide, Q-CNC-1 displayed positive zeta potential from pH 4 to 11, suggesting the successful quaternization of PDMAEMA. The zeta potential still displayed some pH responsiveness due to the deprotonation of un-quaternized tertiary ammonium groups on Q-CNC-1. The size of Q-CNC-1 ranged from 400-550 nm and decreased with the increasing pH due the remaining deprotonated tertiary ammonium groups that were mildly hydrophobic resulting in a reduction in the hydrodynamic radius. Q-CNC-1 shows better dispersity than PDMAEMA-g-CNCs at high pH because the permanent positive charge on quaternary ammonium groups that stabilized the particles. (Fig. 3-5b inset) Similarly, Q-CNC-2 exhibited positive zeta potential among pH 4-11. However, at pH 11, the size of Q-CNC-2 dramatically increased to over 1 micron (Fig. 3-5c inset) The surface charge of Q-CNC-2 at pH 11 was less than +20 mV, which was insufficient to produce a highly stable suspension. The positively charged QA groups and negatively charged sulfate groups on modified CNCs

attracted one another and induced aggregation. The difference in the zeta potential behaviour between Q-CNC-1 and Q-CNC-2 was due to the different degree of quaternization (DQ). It is considered that the quaternizing agent of Q-CNC-2, (2-bromoethyl) benzene, was a larger molecule and thus had higher steric hindrance which led to a lower degree of quaternization. For the same reason, the DQ of Q-CNC-3 was very low and it exhibited the same zeta potential pH responsive patterns as PDMAEMA-g-CNC, hence we hypothesized that the quartenization was not successful. (Fig. 3-5d)

In general, the zeta potentials of Q-CNC can be used to qualitatively evaluate the DQ of PDMAEMA-g-CNCs. As shown in Fig. 3-5d, with higher DQ, the obtained Q-CNC showed higher overall zeta potential and lower pH responsiveness compared to PDMAEMA-g-CNC. Also, for samples with low DQ, aggregation could occur at high pH due to the electrostatic interaction between positively charged QA groups and negatively charged sulfate groups on Q-CNC.

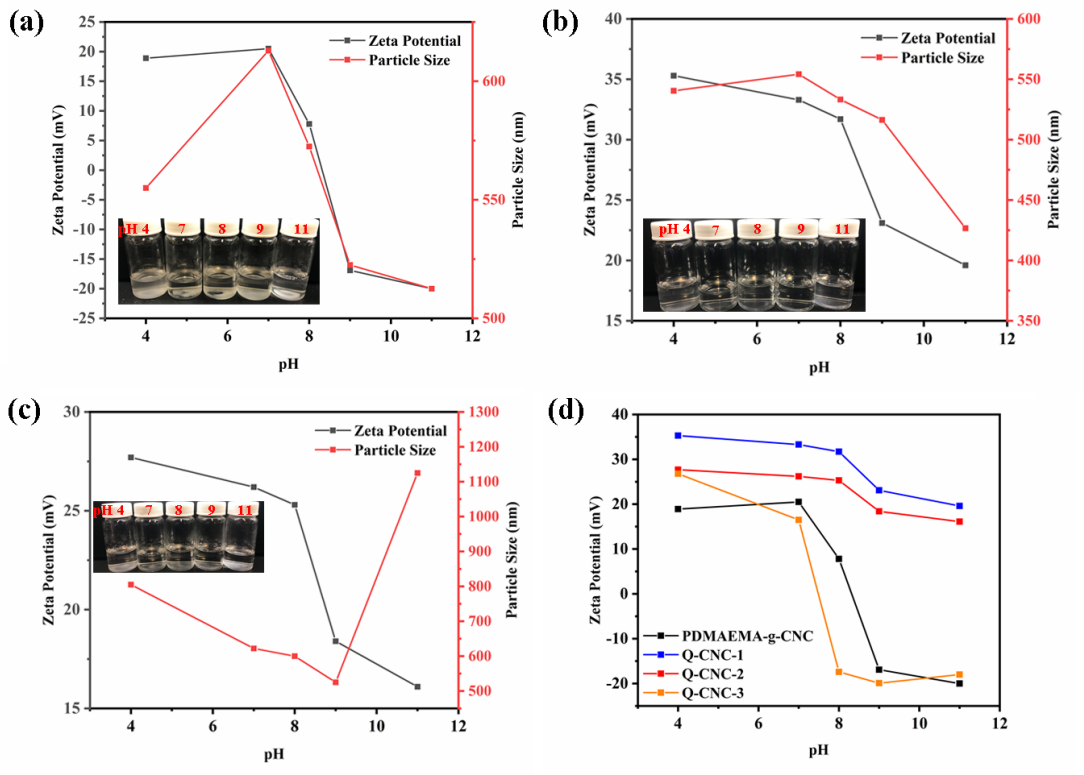

Figure 3-5 Zeta potential and particle size of (a) PDMAEMA-g-CNCs, (b) Q-CNC-1, (c) Q-CNC-2. (d) Zeta potential comparison of PDMAEMA-g-CNCs and 3 different Q-CNC samples.

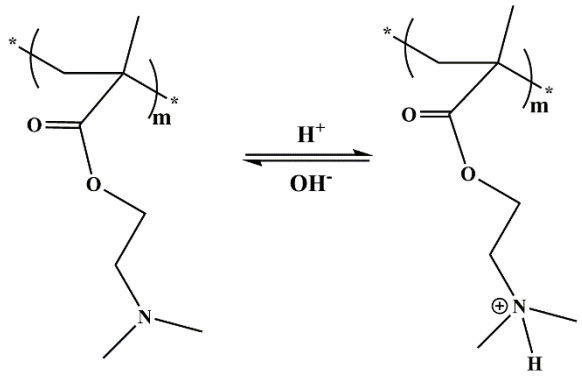

Figure 3-6 Protonation of PDMAEMA side chains at low pH.

3.3.4 Degree of quaternization determined by titration

In the previous section, the DQ of Q-CNC-1 and Q-CNC-2 was qualitatively evaluated by the zeta potential and colloidal stability. In order to quantitatively estimate and compare the DQ using different quaternizing agents, titration tests were performed to determine the amount of tertiary ammonium groups (N_{TA}, mmol/g) and quaternary ammonium groups (N_{QA}, mmol/g) of the prepared samples.

N_{TA} of PDMAEMA-g-CNC was determined using 10 mM NaOH as the titrant. The sample suspension was adjusted to pH 3.6 to ensure the complete protonation of tertiary ammonium groups on PDMAEMA side chains. As shown in Fig. 3-7a, the conductivity displayed three linear regions: 1) sharp decrease, 2) slow increase, and 3) sharp increase. In the first region, at low pH, the suspension showed high conductivity due to the high H^+ concentration which has the highest cation mobility. The addition of NaOH titrant neutralized H^+ ions thereby dramatically reducing the conductivity. In the second stage, NaOH reacted with protonated PDMAEMA (Fig. 3-6) resulting in the deprotonation of tertiary ammonium groups, which maintained the equilibrium of H^+ in the solution. The slow increase of conductivity is caused by the addition of Na^+ cations. In the last linear phase, with the complete deprotonation of tertiary ammonium groups, the H^+/OH^- concentration again became the dominant factor for the conductivity. The rapid increase of OH^- anions led to the sharp increase of conductivity. Therefore, PDMAEMA-g-CNC had an N_{TA} equivalent to the NaOH consumed in the second stage, which could be calculated using Eq. (1). The prepared PDMAEMA-g-CNC had N_{TA} of 4.36 mmol/g.

N_{QA} of Q-CNC was determined using 10 mM $AgNO_3$ as titrant. Fig. 3-7bc shows the titration curve of Q-CNC-1 and Q-CNC-2, respectively. The conductivity change of Q-CNC suspension showed two linear phases. In the first stage, the added Ag^+ quickly reacted with the Br- counter-ion of quaternary ammonium groups on Q-CNC to form a brow precipitate. Therefore, the total ion concentration remained unchanged and the conductivity remained constant. In the second phase, $AgNO_3$ had completely reacted with all the counter-ions and the excess Ag^+ and NO_3^- led to the increase in conductivity. The N_{QA} was calculated by the amount of $AgNO_3$ titrant used in the first linear section using Eq. (2). The resulted N_{QA} for Q-CNC-1 and Q-CNC-2 were 2.18 mmol/g and 1.08 mmol/g, respectively. The titration of Q-CNC-3 did not display the two-phase behavior and the quaternization was thus considered unsuccessful.

Fig. 3-7d shows the N_{TA} of PDMAEMA-g-CNC, N_{QA} of Q-CNC-1 and Q-CNC-2. The DQ of Q-CNC-1 and Q-CNC-2 were 50.0% and 24.8%, respectively. For both Q-CNCs, the DQ was limited due to the steric hindrance of PDMAEMA chains. Due to the larger molecule size of (2-bromoethyl) benzene compared with benzyl bromide, Q-CNC-2 possessed significantly lower DQ. For the same reason, 1-bromo-3-phenylpropane could not quaternize PDMAEMA-g-CNC. The antimicrobial effects of the Q-CNC will be discussed in the following section.

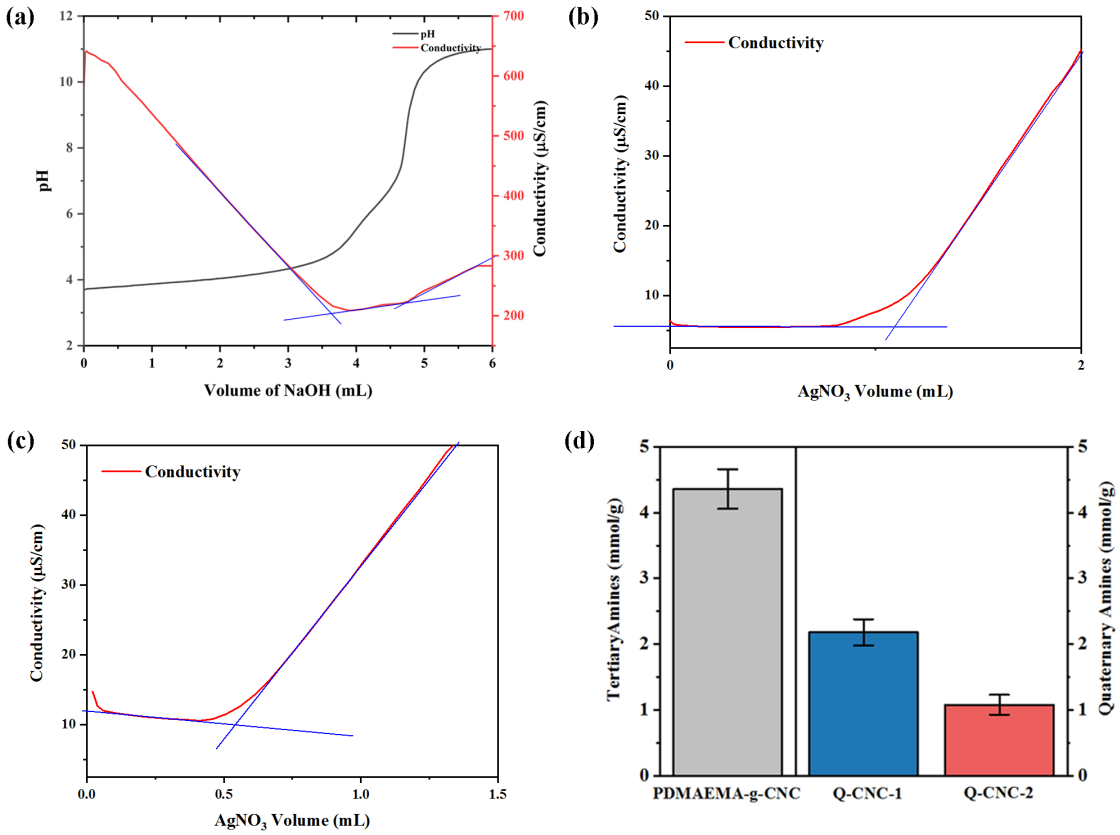

Figure 3-7 Titration results of (a) PDMAEMA-g-CNC by 10 mM NaOH. Titration results of (b) Q-CNC-1 and (c) Q-CNC-2 by 10 mM $AgNO_3$. (d) Titration-determined tertiary ammonium groups and quaternary ammonium groups.

3.3.5 Antimicrobial tests

The antimicrobial activity of synthesized Q-CNC was tested by yeast experiment. In this experiment, suitable environment with pH 6.0, temperature 42 °C, and glucose were used to support the anaerobic metabolism (fermentation) of yeast, which rapidly produced ethanol and CO_2 in the process. By continuously monitoring the CO_2 production of yeast fermentation, the antifungal activity of Q-CNC could be evaluated.

The yeast experiment of un-quaternized PDMAEMA-g-CNC was used as a control experiment. As shown in Fig. 3-8a, the antimicrobial activity of Q-CNC-1 was tested for a concentration gradient ranging from 50 μg/mL to 200 μg/mL. Compared with the control experiment, Q-CNC-1 did not show observable antimicrobial activity at 50 μg/mL and 100 μg/mL. At 150 μg/mL, the CO_2 production had an observable reduction of around 30%, suggesting a partial inhibition of yeast. 200 μg/mL exhibited identical patterns with 150 μg/mL. The further increase in concentration did not led to a higher inhibitory activity. For Q-CNC-2 which had a lower DQ, no observable antimicrobial activity was detected at concentration up to 200 μg/mL. (Fig. 3-8b) Generally, both Q-CNC-1 and Q-CNC-2 did not exhibit expected antimicrobial activities, which could be caused by two major factors: 1) the limited DQ of Q-CNC did not provide enough high concentration of quaternary ammonium groups, 2) the heavily grafted QA polymers and the electrostatic attraction between Q-CNC and yeast led to the aggregation of yeast instead of inhibiting the yeast growth. (Fig. 3-9)

In order to address these problems and improve the antimicrobial activity of Q-CNC, further research was conducted, and it will be discussed in the following chapter.

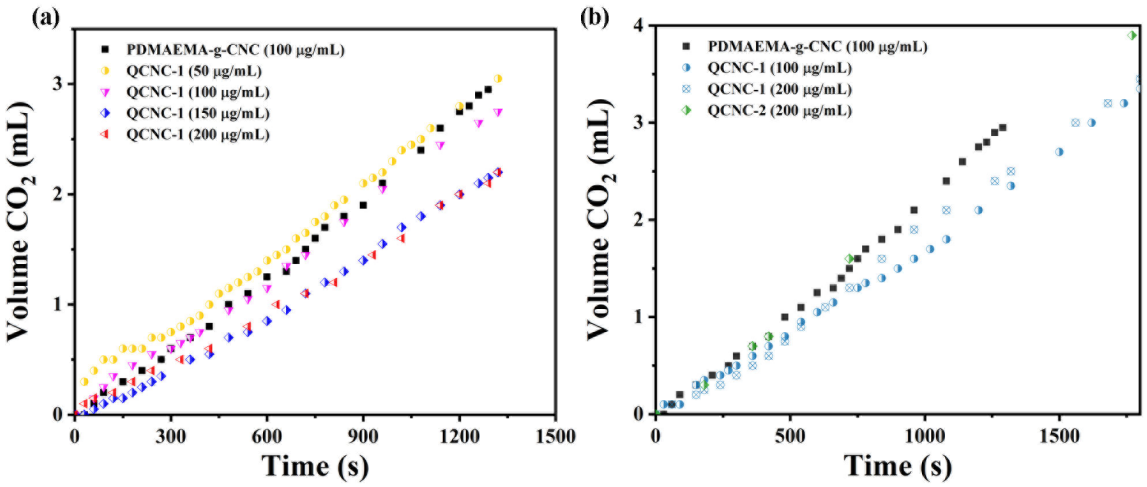

Figure 3-8 Results of yeast experiments of (a) Q-CNC-1 with gradient concentrations.

(b) Comparison between Q-CNC-1 and Q-CNC-2.

Figure 3-9 A photograph of yeast experiment treated with 200 μg/mL Q-CNC-1.

3.4 Conclusion

In this chapter, PDMAEMA-g-CNC was successfully synthesized by surface-initiated ARGET-ATRP. The synthesized PDMAEMA-g-CNC had size ranging from 550-600 nm and exhibited pH-responsive zeta potential from +20 mV to -20 mV due to the protonation and deprotonation of tertiary ammonium groups. The grafted PDMAEMA had N_{TA} of 4.36 mmol/g. Quaternization of PDMAEMA-g-CNC was conducted using three quaternizing agent: benzyl bromide, (2-bromoethyl) benzene, and 1-bromo-3-phenylpropane. The DQ of Q-CNC varied because of the steric hindrance of larger molecules. The Q-CNC-1 and Q-CNC-2 were successfully synthesized with DQs of 50.0% and 24.8%, respectively. The synthesis of Q-CNC-3 was not successful because of the high steric hindrance. In the antimicrobial tests, Q-CNC-1 showed 30% of inhibition at concentrations higher than 150 μg/mL. However, no observable antimicrobial activity of Q-CNC-2 was observed to 200 μg/mL. It is considered that the low DQ and heavily grafted QA polymers lead to poor dispersity of Q-CNCs and thus limited the antimicrobial activity. These problems will be addressed in the following sections.

Chapter 4 Effects of chain density and chain length on polymer grafted CNCs

4.1 Introduction

In chapter 3, PDMAEMA-g-CNC was successfully synthesized by surface-initiated ARGET-ATRP. After quaternization, the QCNCs showed positive surface charge and antimicrobial activity. Moreover, it was found that the high grafting density of PDMAEMA decreased the dispersity of CNCs due to the increased hydrophobicity. Also, the high steric hindrance of heavily grafted CNCs inhibited the quaternization of tertiary ammonium groups with larger molecules leading to a low degree of quaternization, which could reduce the antimicrobial efficiency. Therefore, further study on adjusting the grafting density and molecular weight of surface polymerization on CNCs is needed.

Surface-initiated free radical polymerization (SI-FRP) is the most common approach to graft polymers from CNCs surface, which is convenient and straight-forward.[118, 119] However, this method has poor control over the molecular weight and grafting density of the polymers grafted from the CNC surface. On the other hand, ATRP is a living chain polymerization, and the surface immobilization of initiators allows the control of grafting density in the final CNC products.[125, 135] Moreover, the kinetics of reverse deactivation of ATRP with the presence of Cu(I) metal complex provide predictable molecular weight at a specified initiator/monomer concentration.[122, 124, 137]

In this chapter, PDMAEMA-g-CNCs with controlled grafting density and chain length were synthesized by controlling the initiator and monomer concentrations. The surface charge, functional groups and degree of quaternization of PCNCs with various grafting densities were compared. The antimicrobial activities of prepared QCNCs were evaluated by yeast experiment to optimized this antimicrobial CNCs system.

4.2 Experimental procedure

4.2.1 Immobilization of BIBB initiator on CNCs

1 g CNCs were dried and dispersed in 100mL DMF by ultrasonication for 30 mins. The suspension was transferred to a 250 mL round flask and 4 mL TEA, 3.00 g DMAP were added. The mixture was then transferred to an ice-bath and stirred at 400 rpm under nitrogen for 30 min. Then, different amounts of BIBB (see Table 5) were added dropwise to the reaction mixture. After 24 h, the product was thoroughly washed with ethanol, and then dialyzed against water for 3 days. The resulting CNC-Br was then freeze dried and stored in the fridge.

Table 5. Summary of BIBB used in the experiment.

	Control (from chapter 3)	High density	Low density
Volume of BIBB added (mL)	6.0	4.0	3.0
Sample name	CNC-Br-vhd	CNC-Br-hd	CNC-Br-ld

4.2.2 ARGET-ATRP of DMAEMA using CNC-Br initiator

The details of initiators and amount of DMAEMA used in the experiment is listed in Table 6. First, 400 mg CNC-Br (see Table 6) was dispersed in 40 mL DMF by ultrasonication for 30 min. The suspension was transferred to a 100 mL round flask and 6 mg $CuBr_2$, 24 μL PMDETA and 12 mmol/ 6 mmol DMAEMA (see Table 6) were added. The mixture was then bubbled with dry nitrogen for 1 h to completely remove the remaining oxygen in the system. The suspension was then heated and kept at 60 °C and stirrer was set at 400 rpm. The polymerization was initiated by dropwise addition of 5 mL (10 mg/mL in DMF) ascorbic acid and the reaction was kept at 60 °C for 24 h. After

polymerization, the obtained PDMAEMA-g-CNC was thoroughly washed with THF, ethanol, and water, and then dialyzed against water for 3 days. The synthesized sample was stored in water suspension and part of the sample was freeze-dried for quaternization.

Table 6. Summary of initiators and amount of monomer used in the experiments.

	Control	High brush density		Low brush density	
Initiator used	CNC-Br-vhd	CNC-Br-hd	CNC-Br-hd	CNC-Br-ld	CNC-Br-ld
Chain length	Long	Long	Short	Long	Short
Monomer (mmol)	12.0	12.0	6.0	12.0	6.0
Sample name	PCNC-vhd	PCNC-hd-L	PCNC-hd-S	PCNC-ld-L	PCNC-ld-S

4.2.3 Quaternization of PDMAEMA-g-CNCs

50 mg of each PCNC was dispersed in 9 mL DMSO by ultrasonication and transferred to a 20 mL flask. 1 mL benzyl bromide was then added, and the reaction were kept at room temperature for 24 h. The synthesized Q-CNC was then washed with acetone, ethanol, water and then dialyzed with water for 3 days. The obtained samples were kept in water suspension. According to the different PCNCs used in the reactions (PCNC-vhd, PCNC-hd-L, PCNC-hd-S, PCNC-ld-L, PCNC-ld-S), the subsequently synthesized QCNCs were noted as QCNC-vhd, QCNC-hd-L, QCNC-hd-S, QCNC-ld-L, QCNC-ld-S, respectively.

4.2.4 Physical and chemical characterization

The morphologies of the samples were observed using a Philips CM10 transmission electron microscope at an accelerating voltage of 60 kV. The transmission electron microscopy (TEM) samples were prepared by depositing a droplet of each

sample (0.01 wt %, sonicated in an ice bath) in a copper grid, and the excess water was removed at room temperature. Fourier transform infrared (FTIR) spectrometry was conducted using a PerkinElmer Spectrum Two over the range of 400−4000 cm^{-1} by taking an average of 16 scans (resolution of $4cm^{-1}$) to minimize inaccuracy during the dynamic scanning.

4.2.5 Zeta potential measurement

The average zeta potential measurement was conducted using Zeta-potential analyzer (Nanosizer ZS, Malvern, UK) following the same procedure previously described in Section 3.2.6.

4.2.6 Titration of PDMAEMA-g-CNC and Q-CNCs

The tertiary ammonium groups (N_{TA}, in mmol/g) of PCNCs and the quaternary ammonium groups (N_{QA}, in mmol/g) of QCNCs were calculated by titration of NaOH and $AgNO_3$, respectively. The titrations and calculations followed the same procedure previously described in Section 3.2.7.

4.2.7 Antimicrobial tests using *Saccharomyces cerevisiae* (yeast)

The antimicrobial activity of quaternized PDMAEMA-g-CNC was evaluated using yeast as a model microorganism. The carbon dioxide (CO_2) production of yeast in a 30-min period was measured every 150 seconds to quantitatively compare the inhibitory effect of different Q-CNCs. The experiment setup is shown in Fig. 3-1. 50 mg yeast and 50 mg D-(+)-glucose were dissolved and mixed in 5 mL Milli-Q water (pH 6.0) in a 10 mL flask. After adding CNCs samples, the mixture was move to a water bath at 42 °C with stirring at 300 rpm. The flask was then sealed, and the generated CO_2 was collected and measured using a burette filled with water.

4.3 Results and discussion

In the previous section, PDMAEMA-g-CNC and the quaternized PDMAEMA-g-CNC were prepared to develop a cationic "CNC polymer brush" with quaternary ammonium as effective antimicrobial components. However, with no control of the density and molecular weight, the synthesized Q-CNCs showed limited antimicrobial efficiency due to the poor dispersity and low degree of quaternization (DQ) resulting from the heavily grafted long-chain PDMAEMA polymer. To address these problems, the chain density and molecular weight of the grafted polymer were controlled by modifying the reaction conditions of ARGET-ATRP.

4.3.1 Synthesis of PCNCs with controlled chain density and chain length

PDMAEMA-g-CNC was prepared by surface-initiated ARGET-ATRP using a Cu/PMDETA based catalytic system. The grafting density of PDMAEMA was determined by the density of immobilized BIBB initiator on the CNCs surface. Therefore, by varying the amounts of BIBB used during the grafting of BIBB, the initiator density of CNC-Br was controlled, and the PDMAEMA grafting density was controlled. (Fig. 4-1a) The CNC-Br samples were denoted as CNC-Br-vhd (very high density), CNC-Br-hd (high density), and CNC-Br-ld (low density) according to the amounts of BIBB initiator used (6 mL, 4 mL, and 3 mL respectively). In the previous chapter, CNC-Br-vhd was used to prepared PDMAEMA with very high grafting density and chain length, which however inhibited the quaternization reaction. Therefore, CNC-Br-hd and CNC-Br-ld were prepared to graft less dense PDMAEMA to enhance the dispersity and DQ of the sample. Fig. 4-2 shows the FTIR results of CNC, CNC-Br with different BIBB grafting

densities. The peak at 1744 cm^{-1} is attributed to the C=O stretching vibration of the immobilized BIBB initiator. With the increasing initiator grafting density, the intensity of the peak increases due to the higher amount of C=O presented in the samples. Also, the broad peak ranging from 3100 cm^{-1} to 3600 cm^{-1} indicates the O-H stretching of the hydroxyl groups on pristine CNCs surface. With the further esterification of initiators, the intensity of the O-H peak significantly decreases due to the substitution of hydroxyl groups. These changes in IR transmittance provide evidence for the different grafting density of initiator and the control over polymer chain grafting density.

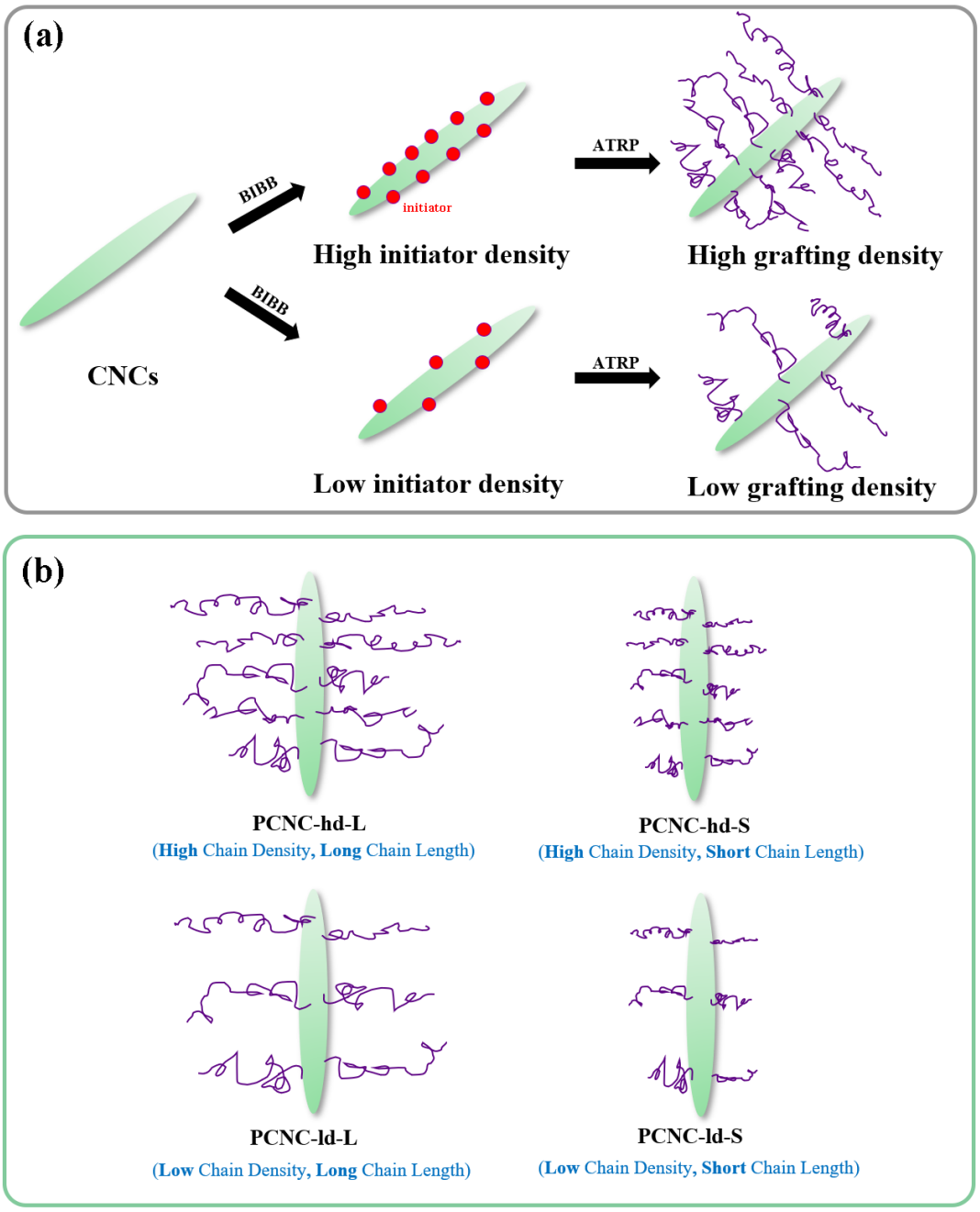

Figure 4-1 (a) A schematic illustration of synthesizing CNC-Br macro-initiators with different initiator densities and the subsequently obtained PCNCs with different grafting densities. (b) A schematic illustration of the expected Q-CNCs with different chain densities and chain lengths.

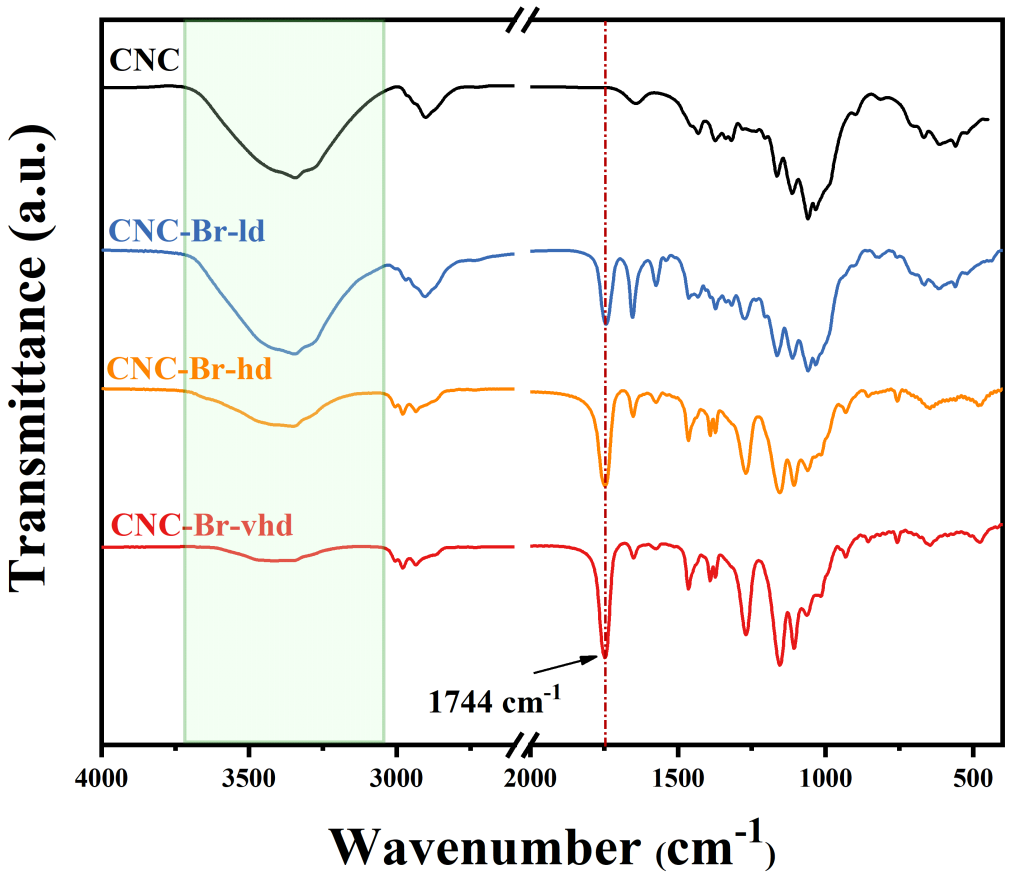

Figure 4-2 FTIR results of CNC (black), CNC-Br-ld (blue), CNC-Br-hd (orange), and CNC-Br-vhd (red).

ATRP is one type of controlled living radical polymerization (CRP), where the initiation, propagation, and chain transfer are reversible with the assistance of the transition metal species (Cu in this case). Due to the characteristics of living chain polymerization, the PDI is usually narrow and the molecular weight has a linear relationship with the monomer conversion. Therefore, given enough polymerization time and the same initiator concentration, the chain length of PDMAEMA can be controlled by the monomer concentration in the reaction. By using two CNC-Br initiators of different chain density and controlling the monomer concentration at 12 mmol and 6 mmol, a total of four PDMAEMA-g-CNC were synthesized. These were designated as

PCNC-hd-L, PCNC-hd-S, PCNC-ld-L, PCNC-ld-S, according to the chain density and chain length of grafted PDMAEMA. (Fig. 4-1b) The previously prepared PDMAEMA-g-CNC in Chapter. 3 was denoted as PCNC-vhd due to the extremely high grafting density and it was used as a control sample in this evaluation.

The PCNCs samples were quaternized using benzyl bromide to ensure a high degree of quaternization (DQ). The characterization of the zeta potential, degree of polymerization, and antimicrobial activity will be discussed in the following sections.

4.3.2 Morphology of prepared PCNCs samples

The TEM images of CNCs and prepared PCNCs are shown in Fig. 4-3. Pristine CNCs extracted via sulfuric acid hydrolysis possessed negative surface charge due to the sulfate ester groups on the surface. Therefore, CNCs showed excellent colloidal stability and individual CNCs had clear edges and the average length of CNCs were around 300 nm. (Fig. 4-3a) TEM image of PCNC-vhd (Fig. 4-3b) showed large, aggregated particles with dimensions over 600 nm due to the heavily grafted PDMAEMA polymers and crosslinks between CNCs, which has been discussed in the previous chapter. PCNC-hd-L and PCNC-hd-S showed very similar morphology with some aggregations and visible rod-shape CNCs with diameters of 300-500 nm. (Fig. 4-3cd) These two samples displayed large particles formed by cross-linked PCNCs, but the edges were much more visible and the thickness of stacked CNCs was much smaller because of the reduced grafting density of PDMAEMA. Similarly, with lower grafting density, PCNC-ld-L and PCNC-ld-S showed better dispersity and smaller particle size, with a diameter of 200-400 nm. (Fig. 4-3ef)

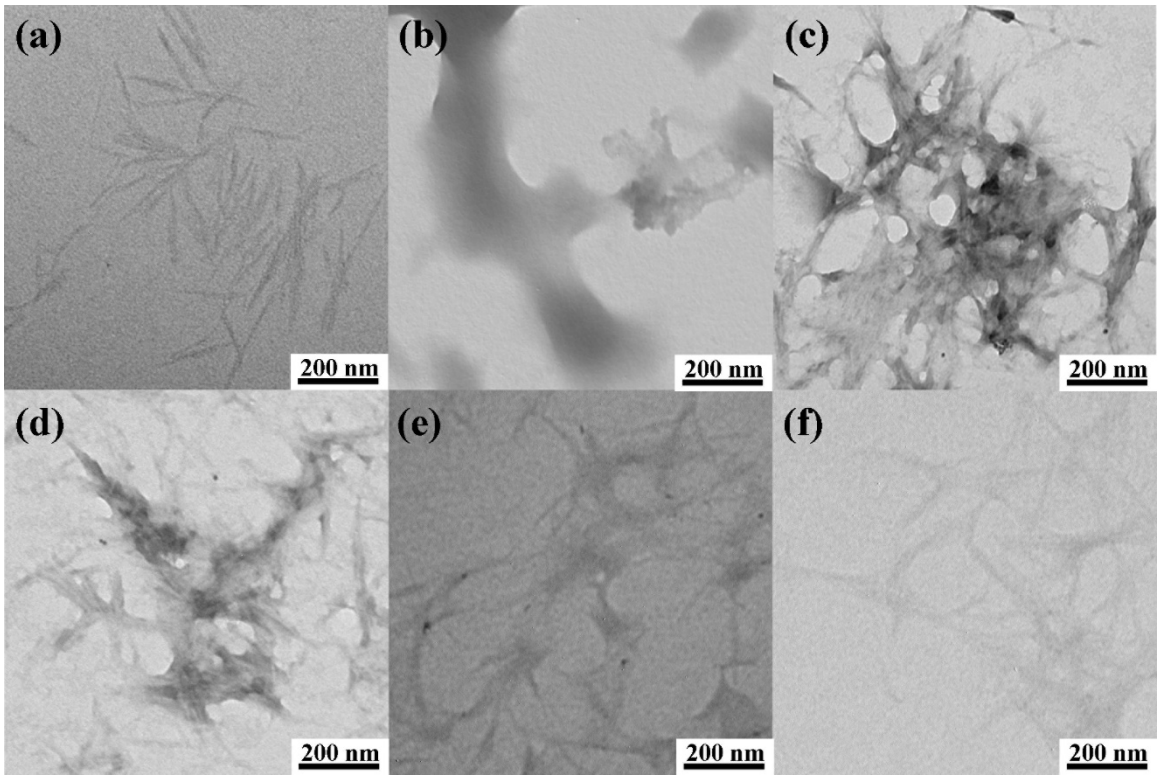

Figure 4-3 TEM image of (a) CNCs, (b) PCNC-vhd, (c) PCNC-hd-L, (d)PCNC-hd-S, (e) PCNC-ld-L, and (f) PCNC-ld-S.

4.3.3 Surface charge of synthesized PCNCs and Q-CNCs

As discussed in the previous chapter, PDMAEMA is a weak polyelectrolyte with a pKa at around 7.4, which makes the surface charge of PDMAEMA-g-CNC pH-responsive due to the protonation and deprotonation of tertiary ammonium groups. (Fig. 3-6) Therefore, as a control experiment, previously synthesized PCNC-vhd possessed zeta potential at around +20 mV at pH ranging from 3 to 7, which decreased to -20 mV at high pH. The zeta potential of PCNC-hd and QCNC-hd are shown in Fig. 4-4a. Both PCNC-hd-L and PCNC-hd-S exhibited similar pH-responsive behavior, which confirmed the successful grafting of PDMAEMA. Both samples showed high zeta potential around

+40 mV at pH 3 and decreased to +25-30 mV at pH 7. At pH 9-11, they were negatively charged because of the complete deprotonation of tertiary ammonium groups while the sulfate groups on CNCs surface remained negatively charged. After quaternization, both QCNC-hd-L and QCNC-hd-S remained positively charged at pH between 3 to 11, suggesting the quaternization was successful. The zeta potential decreased with increasing pH because the unquaternized tertiary ammonium groups deprotonated at high pH and reduced the total amount of positive charges on the surface. Compared with previously synthesized PCNC-vhd, both PCNC-hd-L and PCNC-hd-S possessed higher zeta potential at pH 3, which could be explained that the improved dispersity with the slight reduction in the grafting density.

Fig.4-4b shows the surface charge characteristics of PCNC-ld-L, PCNC-ld-S, and their quaternized samples. The general zeta potential results followed the same pH-responsive behaviour of PCNCs and QCNCs. Compared with PCNC-hd, there are two major difference: 1) At pH 3, both PCNC-ld-L and PCNC-ld-S showed lower zeta potential than PCNC-hd. This was caused by the difference in tertiary ammonium groups on the surface. This trend was also displayed by Q-CNCs with different grafting densities. 2) At pH 11, there was an obvious increase in the zeta potential of PCNCs and QCNCs with lower chain density, which was not observed previously. It is considered that the low chain density made it easier for the base to react with surface sulfate ester groups on the CNC surface.[190] The partial desulfation of CNCs led to the change in net charge of the nanoparticle, which increased the zeta potential but did not affect the total amount of tertiary/ quaternary ammonium groups.

In conclusion, both PCNCs with high chain density and low chain density were successfully synthesized and subsequently quaternized using benzyl bromide. Compared with PCNC-vhd, both PCNC-hd and PCNC-ld showed better dispersity and higher zeta potential at low pH. PCNC-hd generally exhibited higher zeta potential than those of PCNC-ld at pH 4 due to the higher amount of positively charged functional groups, which also yielded the same trend as QCNCs. The low grafting density made it easier for the hydrolysis of sulfate groups on CNCs, which could lead to an increase in zeta potential at pH 11.

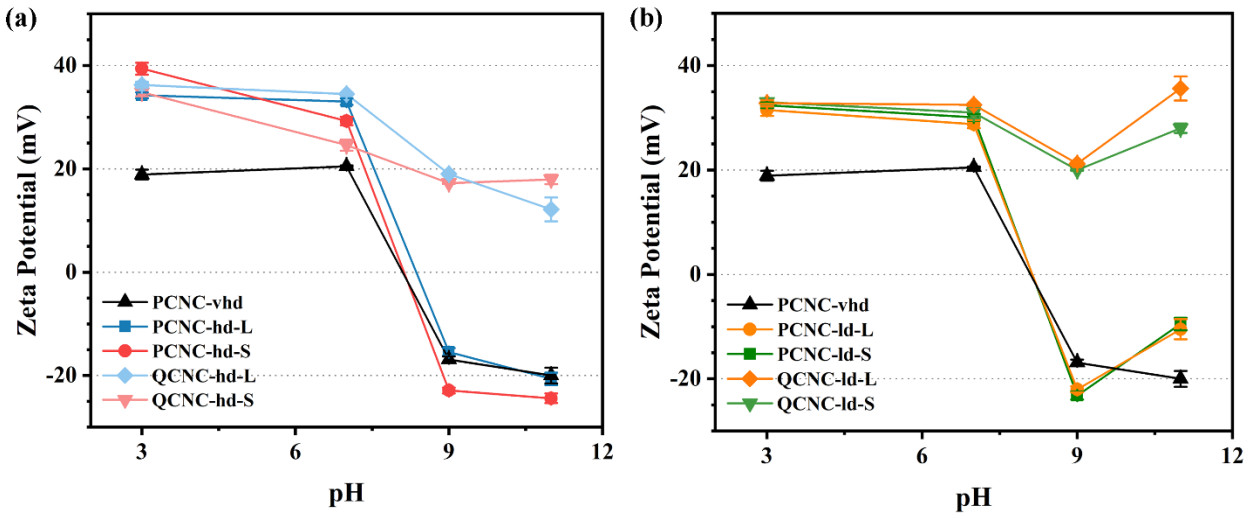

Figure 4-4 Zeta potential of (a) PCNCs and QCNCs with high grafting density, (b) PCNCs and QCNCs with low grafting density.

4.3.4 Degree of quanternization determined by titration

In the previous chapter, PCNC with very high grafting density of PDMAEMA was prepared and quaternized. However, it is considered that the extremely high chain density resulted in poor dispersity and high steric hindrance, which were both unfavorable for achieving a high DQ during the quaternization. Therefore, in this chapter, four different PCNCs with various grafting densities and chain lengths were prepared to investigate the relationship between DQ and polymer grafting on CNCs. In order to quantitatively estimate and compare the DQ for different grafting density and chain length, conductometric titrations were performed to determine the amount of tertiary ammonium groups (N_{TA}, mmol/g) and quaternary ammonium groups (N_{QA}, mmol/g) of the prepared samples.

As previously explained in section 3.3.4, the NaOH titration of PCNCs usually lead to the conductivity change in three different linear regions: 1) sharp decrease, 2) slow increase, and 3) sharp increase. (Fig. 4-5abcd) Briefly, this phenomenon was caused by the effect of deprotonation of tertiary ammonium (TA) groups on the cation/ anion concentration change in the suspension. The sharp change in conductivity resulted from the high mobility of H^+ and OH^- in the solution, while the existence of pH responsive TA groups reacted with NaOH and slowed down the conductivity change. Thus, PCNC had the equivalent N_{TA} as the NaOH consumed in the second stage, which could be calculated using Eq. (1). Similarly, the reaction between halide counter ions on quaternary ammonium groups and Ag^+ precipitated the ions and reduced the conductivity, which could be used to calculate the N_{QA} of a QCNC sample via Eq. (2). (Fig. 4-5ef)

The N_{TA} and N_{QA} of the prepared PCNC, QCNC samples are shown in Fig 4-6a. As a control sample, PCNC-vhd possessed very high grafting density and long chain length, with a high N_{TA} of 4.36 mmol/g. By slightly reducing the amounts of BIBB used in the experiment, PCNC-hd-L and PCNC-hd-S with high grafting density (but lower than the control sample- PCNC-vhd), while PCNC-ld-L and PCNC-ld-S had the lowest polymer chain density. By comparing PCNC-vhd (4.36 mmol/g), PCNC-hd-L (2.92 mmol/g), and PCNC-ld-L (1.68 mmol/g), we observed that with the same amount of monomer used during polymerization, a higher chain density resulted in a higher N_{TA} loading. This is because the heavier the polymers were grafted, the higher mass proportion it took regarding to the total mass of the PCNC. By comparing PCNC-hd-L (2.92 mmol/g) with PCNC-hd-S (1.68 mmol/g), PCNC-hd-S had more than ½ N_{TA} over that of PCNC-hd-L despite the doubling of the molar concentration of monomers used in PCNC-hd-L. Also, the same trend was observed for PCNC-ld-L (0.78 mmol/g) and PCNC-ld-S (0.54 mmol/g), which indicated that the monomers in SI-ATRP of CNCs were not completely consumed. It is considered that the limited space on the CNC surface led to a maximum molecular weight for a given polymer grafting density because of the increasing steric hindrance during the polymerization, which hindered the chain propagation due to steric hindrance.

The DQ of the various QCNCs was calculated using Eq. (3) and shown in Fig. 4-6b. The control sample of previously synthesized QCNC-vhd with very high chain density displayed the lowest DQ of 50.0%. By comparing QCNC-vhd (50%), QCNC-hd-L 73.9%), and QCNC-ld-L (88.0%), it was evident that a lower grafting density of PDMAEMA led to a higher DQ. It is because the high grafting density increased the

steric hindrance of quaternization resulting in a lower yield. Also, by comparing QCNC-hd-L (73.9%) with QCNC-hd-S (64.2%), and QCNC-ld-L (88.0%) with QCNC-ld-S (75.9%), we observed that with the same grafting density, longer chain length of PDMAEMA led to a higher DQ. It is suggested that the side groups of PDMAEMA-g-CNC on longer polymer chains had less steric hindrance and could be quaternized more easily.

In conclusion, the amounts of tertiary ammonium groups on PCNC was determined and calculated by NaOH titration, while the quaternary ammonium groups were determined from $AgNO_3$ titration. It is found that the total N_{TA} decreased with lower grafting density and polymer chain length. Also, we speculated that with the same grafting density, the steric hindrance prevented the complete conversion of monomers. Moreover, the DQ of QCNC is related to both grafting density and chain length. The lower grafting density and longer chain length led to a higher DQ due to the reduced steric hindrance.

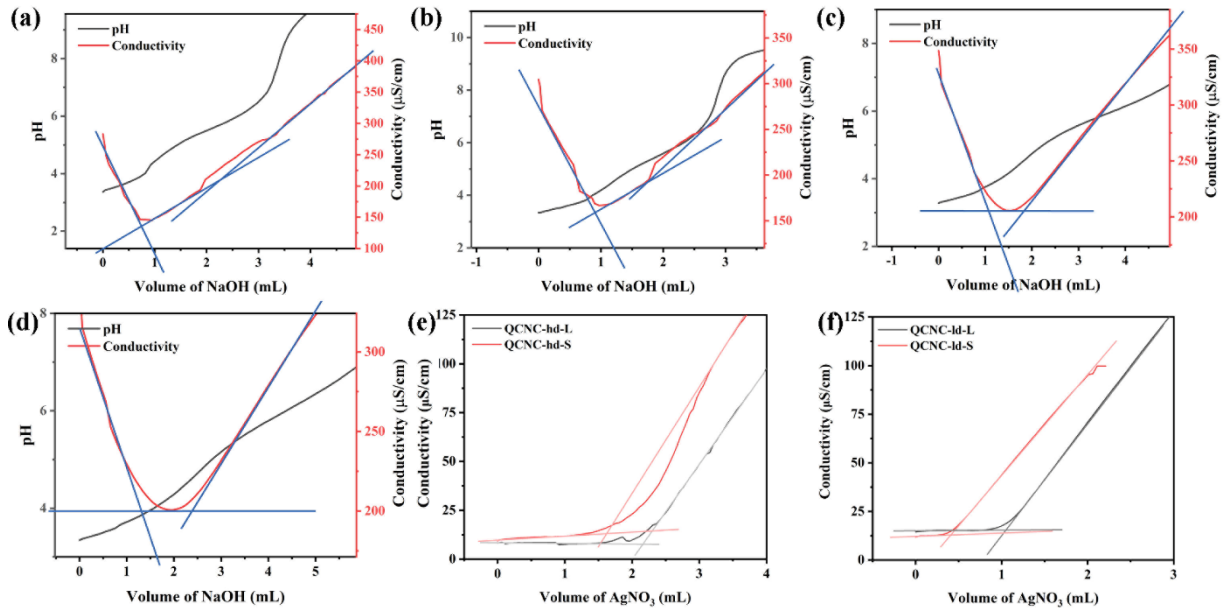

Figure 4-5 Titration curves of (a) PCNC-hd-L, (b) PCNC-hd-L, (c) PCNC-ld-L, and (d) PCNC-ld-S by 10 mM NaOH. Titration curves of (e) QCNC-hd-L and QCNC-hd-S, (f) QCNC-hd-L and QCNC-hd-S by 10 mM $AgNO_3$.

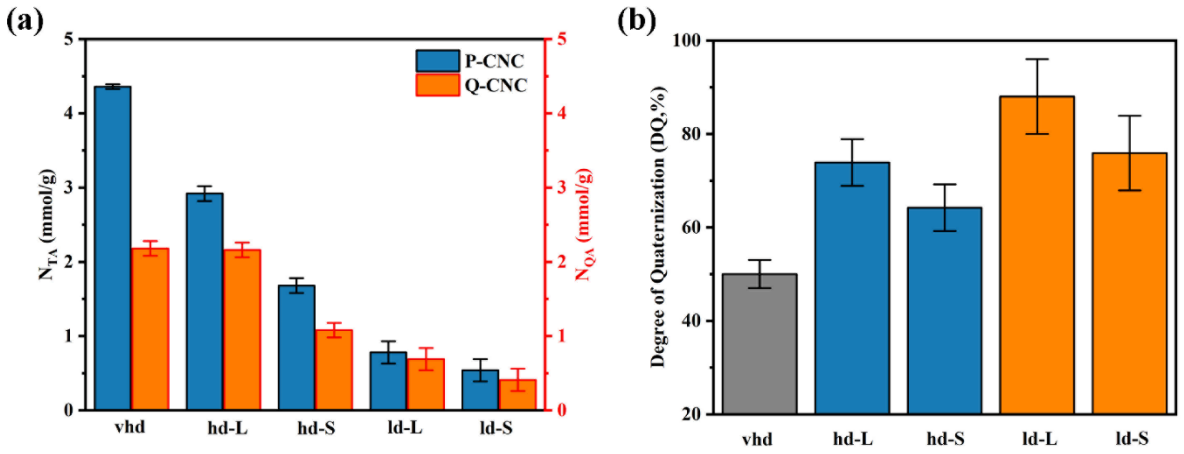

Figure 4-6 (a) N_{TA} and N_{QA} of prepared PCNCs and QCNCs determined by titration. (b) DQ of QCNC samples.

4.3.5 Antimicrobial tests

The antimicrobial activity of d Q-CNC was tested using the yeast experiments. For this experiment, an optimal condition of pH 6.0, temperature 42 °C, and glucose were utilized to support the anaerobic metabolism (fermentation) of yeast, which rapidly produces ethanol and CO_2. By continuously monitoring the CO_2 production of yeast fermentation, the antifungal activity of Q-CNC can be evaluated.

The yeast experiment of un-quaternized PCNCs were used as the control experiments. As shown in Fig. 4-7a, the antimicrobial activity of QCNC-hd-L was tested for a concentration ranging from 100 μg/mL to 1000 μg/mL. Compared to the control experiment, QCNC-hd-L showed a 25% of yeast metabolism inhibition at 100 and 300 μg/mL, 55% at 600 μg/mL, and complete inhibition at 1000 μg/mL. Fig. 4-7b shows the antimicrobial activity of QCNC-hd-S. With shorter polymer chain length, QCNC-hd-S showed 25% inhibition with concentrations up to 1500 μg/mL. At 2000 μg/mL, QCNC-hd-S also fully inhibited the activity of yeast. Fig. 4-7cd shows the antimicrobial activity of QCNC-ld-L and QCNC-ld-S. Both samples did not show complete inhibition of yeast at 2000 μg/mL. Compared with QCNC-ld-S, QCNC-hd-L showed stronger antimicrobial activity, with 68% inhibition at 2000 μg/mL.

However, the antimicrobial activity of QCNC was determined by the effective quaternary ammonium groups in each sample. The measurement of mass minimum inhibitory concentration reflects the overall antimicrobial property of QCNC, but the differential comparison in terms of polymer grafting density and chain length requires the equivalent effective group (QA group) concentration. Figure 4-8 shows the antimicrobial test results of the synthesized QCNC samples with the same quaternary ammonium group

concentration at 10^{-3} mmol. With the same quaternary ammonium group concentration, QCNC-ld-L exhibited the best antimicrobial activity with a 65% inhibition. While QCNC-hd-L showed the second-best antimicrobial efficiency with a 54% inhibition. QCNC-ld-S and QCNC-hd-S showed lower antimicrobial activities with 30% and 20% inhibition, respectively.

Generally, two trends could be observed from the yeast experiments: 1) With the same polymer grafting density, QCNC with longer polymer brush displayed better antimicrobial activities. 2) QCNC with low grafting density showed an overall better antimicrobial efficiency than QCNC with high grafting density. It is considered that the concentration of effective quaternary ammonium groups was the major factor that contributed to the antimicrobial activity of QCNCs. And the antimicrobial activity of QCNC in terms of grafting density and chain length largely consists with the difference in DQ, where QCNC-ld-L showed both highest DQ and best antimicrobial activity at the same QA concentration.

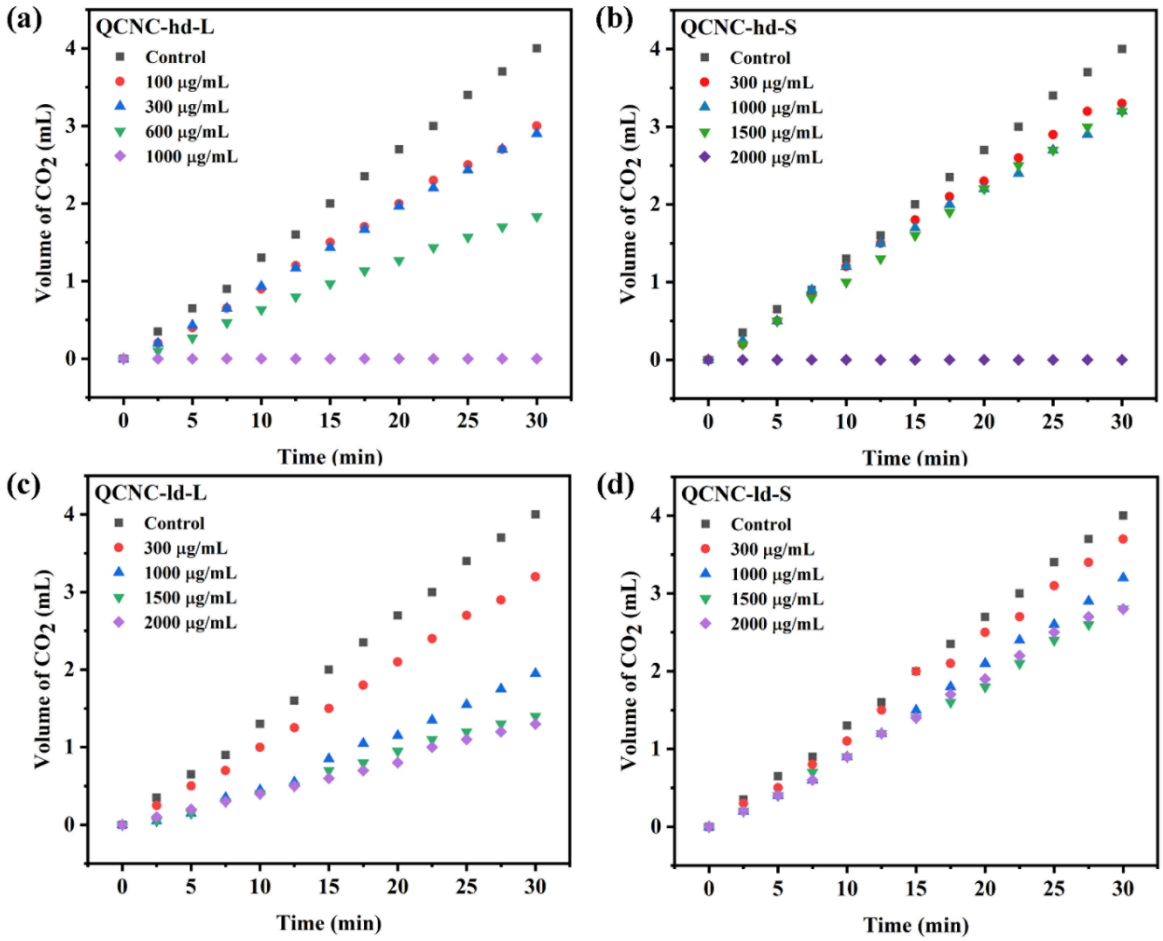

Figure 4-7 Results of yeast experiments of (a) QCNC-hd-L, (b) QCNC-hd-S, (c) QCNC-ld-L, (d) QCNC-ld-S with a concentration gradient.

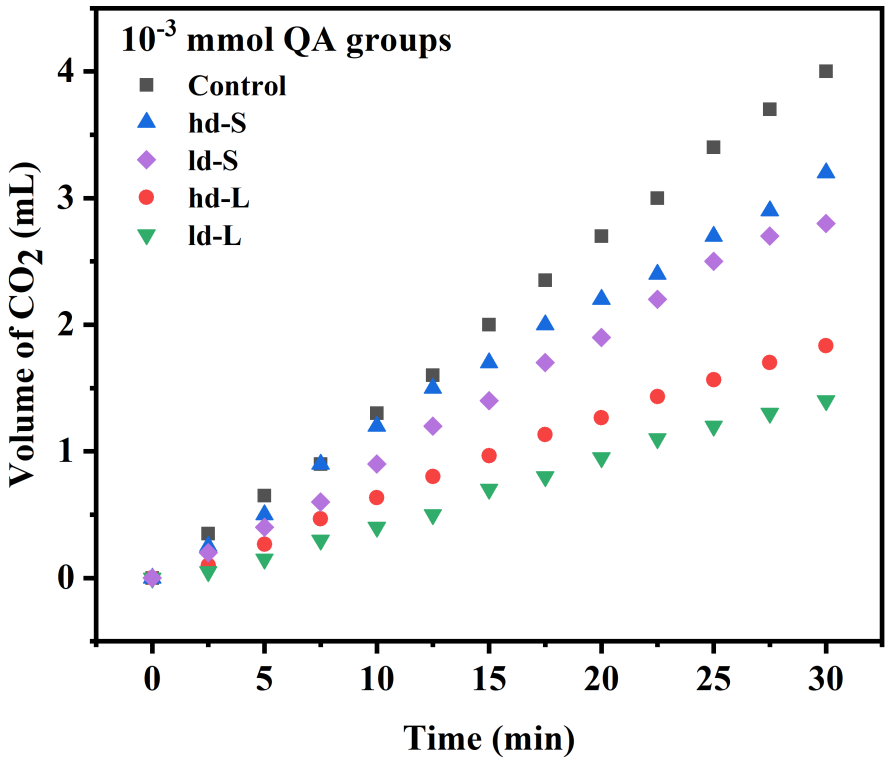

Figure 4-8 Compiled results of yeast experiments of QCNC samples at 10^{-3} mmol quaternary ammonium groups concentration.

4.4 Conclusions

In this chapter, PDMAEMA-g-CNCs with controlled grafting density and chain length were synthesized. A total of 4 samples, namely, PCNC-hd-L, PCNC-hd-S, PCNC-ld-L, and PCNC-ld-S were successfully prepared by ARGET-ATRP using CNC-Br macro-initiators synthesized with reduced grafting density. The prepared PCNCs were subsequently quaternized using benzyl bromide. The prepared PCNCs samples showed pH responsive zeta potential ranging from +40 to -20 mV from pH 3-11, while the quaternized QCNCs exhibited permanent positive charge among all pH, indicating the successful quaternization. The DQ of the prepared QCNCs for the different grafting density and chain length of PDMAEMA were studied by conductometric and silver nitrate titrations. Among them, QCNC-ld-L showed the highest DQ of 88% with N_{TA} of 0.78 mmol/g and N_{QA} of 0.69 mmol/g. It was discovered that the total N_{TA} decreased with lower grafting density and polymer chain length and the lower grafting density and longer chain length led to higher DQ due to the decreased steric hindrance. In the yeast experiments, QCNC-ld-L possessed the best antimicrobial activity with a MIC of 1000 μg/mL. However, with the same quaternary ammonium group concentration, QCNC-ld-L showed the best antimicrobial activity, which consist with the highest DQ of this sample. It is considered that the antimicrobial activity was closely related to the concentration of effective groups on QCNCs. Also, at the same effective group concentration, QCNC with low grafting density and long chain length showed better antimicrobial activity.

Chapter 5 Conclusions and plans for future study

In summary, CNC based antimicrobial nanomaterials were successfully prepared by grafting poly(diethylaminoethyl methacrylate) (PDMAEMA) via surface-initiated ARGET-ATRP and quaternizing the grafted polymer chains. The grafting density and molecular weight of the PDMAEMA-g-CNC were controlled by adjusting the surface initiator immobilization and monomer concentrations. After polymer grafting, the obtained PCNCs showed pH responsiveness due to the protonation of tertiary ammonium functional groups. These samples were subsequently quaternized to obtain quaternary ammonium polymer grafted CNCs. The degree of quaternization of different PDMAEMA-g-CNCs with various grafting density and chain length were evaluated by titration, and the antimicrobial activity was tested. It was found that smaller quaternizing agents, lower chain density and longer chain length led to a higher degree of quaternization that enhanced the antimicrobial activity of the Q(PDMAEMA)-g-CNC, up to 88% with N_{TA} of 0.78 mmol/g and N_{QA} of 0.69 mmol/g. Consistent with the DQ results, QCNC-ld-L displayed the best antimicrobial activity with a 65% of inhibition at 10^{-3} mmol QA concentration. It is considered that in this QA polymer grafted CNCs system, low grafting density and long chain length improve the antimicrobial activity of the CNC. These findings could be applied to optimize the CNC ATRP surface grafting systems and they could be potentially used in applications, such as Pickering emulsion, antimicrobial and drug delivery.

It is recommended that a quantitative measurement of initiator grafting density and polymer molecular weight can be performed to achieve a more precise control of the grafted polymer. Due to the poor dispersity of pristine CNCs in most organic solvents, it

is suggested that an alternative solvent-free method for initiator immobilization can be studied. Also, pre-treatment of CNCs or post-treatment of PCNCs can be performed to remove the negatively charged sulfate groups on CNCs to further improve the stability and antimicrobial activity of this system. Apart from this, further studies on the hydrophobicity and antimicrobial activity can be investigated. In the future work, more quaternizing agents (organic halides) can be tested to optimize the DQ and antimicrobial activity of this systems.

References

1. Amaral, P. E. M.; Hall, D. C.; Pai, R.; Król, J. E.; Kalra, V.; Ehrlich, G. D.; Ji, H.-F., Fibrous Phosphorus Quantum Dots for Cell Imaging. *ACS Applied Nano Materials* **2020,** *3* (1), 752-759.
2. Dairi, N.; Ferfera-Harrar, H.; Ramos, M.; Garrigos, M. C., Cellulose acetate/AgNPs-organoclay and/or thymol nano-biocomposite films with combined antimicrobial/antioxidant properties for active food packaging use. *Int J Biol Macromol* **2019,** *121*, 508-523.
3. Duncan, T. V., Applications of nanotechnology in food packaging and food safety: barrier materials, antimicrobials and sensors. *J Colloid Interface Sci* **2011,** *363* (1), 1-24.
4. Fang, R.; Chen, K.; Yin, L.; Sun, Z.; Li, F.; Cheng, H. M., The Regulating Role of Carbon Nanotubes and Graphene in Lithium-Ion and Lithium-Sulfur Batteries. *Adv Mater* **2019,** *31* (9), e1800863.
5. Gao, F.; Qiu, Y.; Wei, S.; Yang, H.; Zhang, J.; Hu, P., Graphene nanoparticle strain sensors with modulated sensitivity through tunneling types transition. *Nanotechnology* **2019,** *30* (42), 425501.
6. Gao, L.; Quan, L. N.; García de Arquer, F. P.; Zhao, Y.; Munir, R.; Proppe, A.; Quintero-Bermudez, R.; Zou, C.; Yang, Z.; Saidaminov, M. I.; Voznyy, O.; Kinge, S.; Lu, Z.; Kelley, S. O.; Amassian, A.; Tang, J.; Sargent, E. H., Efficient near-infrared light-emitting diodes based on quantum dots in layered perovskite. *Nature Photonics* **2020,** *14* (4), 227-233.
7. Giraldo, J. P.; Wu, H.; Newkirk, G. M.; Kruss, S., Nanobiotechnology approaches for engineering smart plant sensors. *Nat Nanotechnol* **2019,** *14* (6), 541-553.
8. Guo, A.; Chen, E.; Wygant, B. R.; Heller, A.; Mullins, C. B., Lead Oxide Microparticles Coated by Ethylenediamine-Cross-Linked Graphene Oxide for Lithium Ion Battery Anodes. *ACS Applied Energy Materials* **2019,** *2* (5), 3017-3020.
9. Hu, W.; Wan, L.; Jian, Y.; Ren, C.; Jin, K.; Su, X.; Bai, X.; Haick, H.; Yao, M.; Wu, W., Electronic Noses: From Advanced Materials to Sensors Aided with Data Processing. *Advanced Materials Technologies* **2018**.
10. Inshakova, E.; Inshakova, A., Nanomaterials and nanotechnology: prospects for technological re-equipment in the power engineering industry. *IOP Conf. Series: Materials Science and Engineering* **2020,** *709* 033020.
11. Kagan, C. R.; Lifshitz, E.; Sargent, E. H.; Talapin, D. V., Building devices from colloidal quantum dots. *Science* **2016,** *353* (6302).
12. Liu, H.; Li, C.; Qian, Y.; Hu, L.; Fang, J.; Tong, W.; Nie, R.; Chen, Q.; Wang, H., Magnetic-induced graphene quantum dots for imaging-guided photothermal therapy in the second near-infrared window. *Biomaterials* **2020,** *232*, 119700.
13. Qu, X.; Alvarez, P. J.; Li, Q., Applications of nanotechnology in water and wastewater treatment. *Water Res* **2013,** *47* (12), 3931-46.
14. Wang, X.; Guo, Z.; Zhang, C.; Zhu, S.; Li, L.; Gu, Z.; Zhao, Y., Ultrasmall BiOI Quantum Dots with Efficient Renal Clearance for Enhanced Radiotherapy of Cancer. *Adv Sci (Weinh)* **2020,** *7* (6), 1902561.
15. Ge, X.; Xia, Z.; Guo, S., Recent Advances on Black Phosphorus for Biomedicine and Biosensing. *Advanced Functional Materials* **2019,** *29* (29).
16. Zheng, X. T.; Goh, W. L.; Yeow, P.; Lane, D. P.; Ghadessy, F. J.; Tan, Y. N., Ultrasensitive dynamic light scattering based nanobiosensor for rapid anticancer drug screening. *Sensors and Actuators B: Chemical* **2019,** *279*, 79-86.
17. El-Sawy, H. S.; Al-Abd, A. M.; Ahmed, T. A.; El-Say, K. M.; Torchilin, V. P., Stimuli-Responsive Nano-Architecture Drug-Delivery Systems to Solid Tumor Micromilieu: Past, Present, and Future Perspectives. *ACS Nano* **2018,** *12* (11), 10636-10664.

18. Manzano, M.; Vallet‐Regí, M., Mesoporous Silica Nanoparticles for Drug Delivery. *Advanced Functional Materials* **2019,** *30* (2).
19. Rai, M.; Yadav, A.; Gade, A., Silver nanoparticles as a new generation of antimicrobials. *Biotechnol Adv* **2009,** *27* (1), 76-83.
20. Holt, K. B.; Bard, A. J., Interaction of Silver(I) Ions with the Respiratory Chain of Escherichia coli:An Electrochemical and Scanning Electrochemical Microscopy Study of the Antimicrobial Mechanism of Micromolar Ag+. *Biochemistry* **2005,** *44*, 13214-13223.
21. Kim, J. S.; Kuk, E.; Yu, K. N.; Kim, J. H.; Park, S. J.; Lee, H. J.; Kim, S. H.; Park, Y. K.; Park, Y. H.; Hwang, C. Y.; Kim, Y. K.; Lee, Y. S.; Jeong, D. H.; Cho, M. H., Antimicrobial effects of silver nanoparticles. *Nanomedicine* **2007,** *3* (1), 95-101.
22. Jung, W. K.; Koo, H. C.; Kim, K. W.; Shin, S.; Kim, S. H.; Park, Y. H., Antibacterial activity and mechanism of action of the silver ion in Staphylococcus aureus and Escherichia coli. *Appl Environ Microbiol* **2008,** *74* (7), 2171-8.
23. Park, H. J.; Kim, J. Y.; Kim, J.; Lee, J. H.; Hahn, J. S.; Gu, M. B.; Yoon, J., Silver-ion-mediated reactive oxygen species generation affecting bactericidal activity. *Water Res* **2009,** *43* (4), 1027-32.
24. Maneerung, T.; Tokura, S.; Rujiravanit, R., Impregnation of silver nanoparticles into bacterial cellulose for antimicrobial wound dressing. *Carbohydrate Polymers* **2008,** *72* (1), 43-51.
25. Lok, C. N.; Ho, C. M.; Chen, R.; He, Q. Y.; Yu, W. Y.; Sun, H.; Tam, P. K.; Chiu, J. F.; Che, C. M., Silver nanoparticles: partial oxidation and antibacterial activities. *J Biol Inorg Chem* **2007,** *12* (4), 527-34.
26. Stankus, D. P.; Lohse, S. E.; Hutchison, J. E.; Nason, J. A., Interactions between natural organic matter and gold nanoparticles stabilized with different organic capping agents. *Environ Sci Technol* **2011,** *45* (8), 3238-44.
27. Abdel-Raouf, N.; Al-Enazi, N. M.; Ibraheem, I. B. M., Green biosynthesis of gold nanoparticles using Galaxaura elongata and characterization of their antibacterial activity. *Arabian Journal of Chemistry* **2017,** *10*, S3029-S3039.
28. Singh, A. K.; Viswanath, V.; Janu, V. C., Synthesis, effect of capping agents, structural, optical and photoluminescence properties of ZnO nanoparticles. *Journal of Luminescence* **2009,** *129* (8), 874-878.
29. Khan, S. T.; Al-Khedhairy, A. A.; Musarrat, J., ZnO and TiO2 nanoparticles as novel antimicrobial agents for oral hygiene: a review. *Journal of Nanoparticle Research* **2015,** *17* (6).
30. Dobrucka, R.; Dlugaszewska, J., Biosynthesis and antibacterial activity of ZnO nanoparticles using Trifolium pratense flower extract. *Saudi J Biol Sci* **2016,** *23* (4), 517-23.
31. Ghasemi, N.; Jamali-Sheini, F.; Zekavati, R., CuO and Ag/CuO nanoparticles: Biosynthesis and antibacterial properties. *Materials Letters* **2017,** *196*, 78-82.
32. Nabila, M. I.; Kannabiran, K., Biosynthesis, characterization and antibacterial activity of copper oxide nanoparticles (CuO NPs) from actinomycetes. *Biocatalysis and Agricultural Biotechnology* **2018,** *15*, 56-62.
33. Rahimi, M.; Hosseini; M.R.; BaNhshi, M.; Baghbanan, A., Biosynthesis of Silver-Phosphate Nanoparticles Using the Extracellular Polymeric Substance of Sporosarcina pasteurii. *International Journal of Biotechnology and Bioengineering* **2017,** *11*, 120-123.
34. Seyfi, J.; Panahi-Sarmad, M.; OraeiGhodousi, A.; Goodarzi, V.; Khonakdar, H. A.; Asefnejad, A.; Shojaei, S., Antibacterial superhydrophobic polyvinyl chloride surfaces via the improved phase separation process using silver phosphate nanoparticles. *Colloids Surf B Biointerfaces* **2019,** *183*, 110438.

35. Taheri, P.; Khajeh-Amiri, A., Antibacterial cotton fabrics via immobilizing silver phosphate nanoparticles onto the chitosan nanofiber coating. *Int J Biol Macromol* **2020,** *158*, 282-289.
36. Abinaya, C.; Marikkannan, M.; Manikandan, M.; Mayandi, J.; Suresh, P.; Shanmugaiah, V.; Ekstrum, C.; Pearce, J. M., Structural and optical characterization and efficacy of hydrothermal synthesized Cu and Ag doped zinc oxide nanoplate bactericides. *Materials Chemistry and Physics* **2016,** *184*, 172-182.
37. Alizadeh, R.; Kashkoei, P. K.; Kazemipour, M., Zinc oxide-copper oxide nanoplates composite as coating for solid phase microextraction combined with high performance liquid chromatography-UV detection for trace analysis of chlorophenols in water and tomato juice samples. *Anal Bioanal Chem* **2016,** *408* (14), 3727-36.
38. Cai, Q.; Gao, Y.; Gao, T.; Lan, S.; Simalou, O.; Zhou, X.; Zhang, Y.; Harnoode, C.; Gao, G.; Dong, A., Insight into Biological Effects of Zinc Oxide Nanoflowers on Bacteria: Why Morphology Matters. *ACS Appl Mater Interfaces* **2016,** *8* (16), 10109-20.
39. Wang, J. X.; Zhuo, Y.; Zhou, Y.; Wang, H. J.; Yuan, R.; Chai, Y. Q., Ceria Doped Zinc Oxide Nanoflowers Enhanced Luminol-Based Electrochemiluminescence Immunosensor for Amyloid-beta Detection. *ACS Appl Mater Interfaces* **2016,** *8* (20), 12968-75.
40. Ullah, S.; Ahmad, A.; Ri, H.; Khan, A. U.; Khan, U. A.; Yuan, Q., Green synthesis of catalytic Zinc Oxide nano-flowers and their bacterial infection therapy. *Applied Organometallic Chemistry* **2019,** *34* (1).
41. Loo, C. Y.; Rohanizadeh, R.; Young, P. M.; Traini, D.; Cavaliere, R.; Whitchurch, C. B.; Lee, W. H., Combination of Silver Nanoparticles and Curcumin Nanoparticles for Enhanced Anti-biofilm Activities. *J Agric Food Chem* **2016,** *64* (12), 2513-22.
42. Adahoun, M. A.; Al-Akhras, M. H.; Jaafar, M. S.; Bououdina, M., Enhanced anti-cancer and antimicrobial activities of curcumin nanoparticles. *Artif Cells Nanomed Biotechnol* **2017,** *45* (1), 98-107.
43. Shi, Z.; Neoh, K. G.; Kang, E. T.; Wang, W., Antibacterial and mechanical properties of bone cement impregnated with chitosan nanoparticles. *Biomaterials* **2006,** *27* (11), 2440-9.
44. Anitha, A.; Divya Rani, V. V.; Krishna, R.; Sreeja, V.; Selvamurugan, N.; Nair, S. V.; Tamura, H.; Jayakumar, R., Synthesis, characterization, cytotoxicity and antibacterial studies of chitosan, O-carboxymethyl and N,O-carboxymethyl chitosan nanoparticles. *Carbohydrate Polymers* **2009,** *78* (4), 672-677.
45. Wu, T.; Wu, C.; Fu, S.; Wang, L.; Yuan, C.; Chen, S.; Hu, Y., Integration of lysozyme into chitosan nanoparticles for improving antibacterial activity. *Carbohydr Polym* **2017,** *155*, 192-200.
46. Du, W.-L.; Niu, S.-S.; Xu, Y.-L.; Xu, Z.-R.; Fan, C.-L., Antibacterial activity of chitosan tripolyphosphate nanoparticles loaded with various metal ions. *Carbohydrate Polymers* **2009,** *75* (3), 385-389.
47. Wei, D.; Sun, W.; Qian, W.; Ye, Y.; Ma, X., The synthesis of chitosan-based silver nanoparticles and their antibacterial activity. *Carbohydr Res* **2009,** *344* (17), 2375-82.
48. Khan, S. B.; Ali, F.; Kamal, T.; Anwar, Y.; Asiri, A. M.; Seo, J., CuO embedded chitosan spheres as antibacterial adsorbent for dyes. *Int J Biol Macromol* **2016,** *88*, 113-9.
49. Biao, L.; Tan, S.; Wang, Y.; Guo, X.; Fu, Y.; Xu, F.; Zu, Y.; Liu, Z., Synthesis, characterization and antibacterial study on the chitosan-functionalized Ag nanoparticles. *Mater Sci Eng C Mater Biol Appl* **2017,** *76*, 73-80.
50. Pereira, A.; Reis, D. T.; Barbosa, K. M.; Scheidt, G. N.; da Costa, L. S.; Santos, L. S. S., Antibacterial effects and ibuprofen release potential using chitosan microspheres loaded with silver nanoparticles. *Carbohydr Res* **2020,** *488*, 107891.

51. Moritz, M.; Geszke-Moritz, M., The newest achievements in synthesis, immobilization and practical applications of antibacterial nanoparticles. *Chemical Engineering Journal* **2013,** *228*, 596-613.
52. Ayesh, A. I.; Ahmed, H. A.; Awwad, F.; Abu-Eishah, S. I.; Mahmood, S. T., Mechanisms of Ti nanocluster formation by inert gas condensation. *Journal of Materials Research* **2013,** *28* (18), 2622-2628.
53. Husanu, E.; Chiappe, C.; Bernardini, A.; Cappello, V.; Gemmi, M., Synthesis of colloidal Ag nanoparticles with citrate based ionic liquids as reducing and capping agents. *Colloids and Surfaces A: Physicochemical and Engineering Aspects* **2018,** *538*, 506-512.
54. Chen, X.; Wei, M.; Jiang, S.; Forster, S., Two Growth Mechanisms of Thiol-Capped Gold Nanoparticles Controlled by Ligand Chemistry. *Langmuir* **2019,** *35* (37), 12130-12138.
55. Lv, Q.; Zhang, B.; Xing, X.; Zhao, Y.; Cai, R.; Wang, W.; Gu, Q., Biosynthesis of copper nanoparticles using Shewanella loihica PV-4 with antibacterial activity: Novel approach and mechanisms investigation. *J Hazard Mater* **2018,** *347*, 141-149.
56. Raja, S.; Ramesh, V.; Thivaharan, V., Green biosynthesis of silver nanoparticles using Calliandra haematocephala leaf extract, their antibacterial activity and hydrogen peroxide sensing capability. *Arabian Journal of Chemistry* **2017,** *10* (2), 253-261.
57. Azocar, M. I.; Alarcon, R.; Castillo, A.; Blamey, J. M.; Walter, M.; Paez, M., Capping of silver nanoparticles by anti-inflammatory ligands: Antibacterial activity and superoxide anion generation. *J Photochem Photobiol B* **2019,** *193*, 100-108.
58. Hu, S.; Hsieh, Y. L., Silver nanoparticle synthesis using lignin as reducing and capping agents: A kinetic and mechanistic study. *Int J Biol Macromol* **2016,** *82*, 856-62.
59. Li, W. R.; Xie, X. B.; Shi, Q. S.; Zeng, H. Y.; Ou-Yang, Y. S.; Chen, Y. B., Antibacterial activity and mechanism of silver nanoparticles on Escherichia coli. *Appl Microbiol Biotechnol* **2010,** *85* (4), 1115-22.
60. Mosselhy, D. A.; El-Aziz, M. A.; Hanna, M.; Ahmed, M. A.; Husien, M. M.; Feng, Q., Comparative synthesis and antimicrobial action of silver nanoparticles and silver nitrate. *Journal of Nanoparticle Research* **2015,** *17* (12).
61. Xu, H.; Qu, F.; Xu, H.; Lai, W.; Andrew Wang, Y.; Aguilar, Z. P.; Wei, H., Role of reactive oxygen species in the antibacterial mechanism of silver nanoparticles on Escherichia coli O157:H7. *Biometals* **2012,** *25* (1), 45-53.
62. Duran, N.; Duran, M.; de Jesus, M. B.; Seabra, A. B.; Favaro, W. J.; Nakazato, G., Silver nanoparticles: A new view on mechanistic aspects on antimicrobial activity. *Nanomedicine* **2016,** *12* (3), 789-799.
63. Bao, H.; Yu, X.; Xu, C.; Li, X.; Li, Z.; Wei, D.; Liu, Y., New toxicity mechanism of silver nanoparticles: promoting apoptosis and inhibiting proliferation. *PLoS One* **2015,** *10* (3), e0122535.
64. Dong, F.; Zhou, Y., Differential transformation and antibacterial effects of silver nanoparticles in aerobic and anaerobic environment. *Nanotoxicology* **2019,** *13* (3), 339-353.
65. Environment, D.; Council, D. E.; Council, D. C. THE NANODATABASE. http://nanodb.dk/en/search-database/.
66. Donner, E.; Scheckel, K.; Sekine, R.; Popelka-Filcoff, R. S.; Bennett, J. W.; Brunetti, G.; Naidu, R.; McGrath, S. P.; Lombi, E., Non-labile silver species in biosolids remain stable throughout 50 years of weathering and ageing. *Environ Pollut* **2015,** *205*, 78-86.
67. Wang, P.; Menzies, N. W.; Dennis, P. G.; Guo, J.; Forstner, C.; Sekine, R.; Lombi, E.; Kappen, P.; Bertsch, P. M.; Kopittke, P. M., Silver Nanoparticles Entering Soils via the Wastewater-Sludge-Soil Pathway Pose Low Risk to Plants but Elevated Cl Concentrations Increase Ag Bioavailability. *Environ Sci Technol* **2016,** *50* (15), 8274-81.

68. Civardi, C.; Schwarze, F. W.; Wick, P., Micronized copper wood preservatives: an efficiency and potential health risk assessment for copper-based nanoparticles. *Environ Pollut* **2015,** *200*, 126-32.
69. León-Silva, S.; Fernández-Luqueño, F.; López-Valdez, F., Silver Nanoparticles (AgNP) in the Environment: a Review of Potential Risks on Human and Environmental Health. *Water, Air, & Soil Pollution* **2016,** *227* (9).
70. Marambio-Jones, C.; Hoek, E. M. V., A review of the antibacterial effects of silver nanomaterials and potential implications for human health and the environment. *Journal of Nanoparticle Research* **2010,** *12* (5), 1531-1551.
71. Pelin, M.; Sosa, S.; Prato, M.; Tubaro, A., Occupational exposure to graphene based nanomaterials: risk assessment. *Nanoscale* **2018,** *10* (34), 15894-15903.
72. Trache, D.; Hussin, M. H.; Haafiz, M. K.; Thakur, V. K., Recent progress in cellulose nanocrystals: sources and production. *Nanoscale* **2017,** *9* (5), 1763-1786.
73. Insights, F. B. *Cellulose Market Size, Share & Industry Analysis, By Derivative Type (Commodity Cellulose Pulp, Cellulose Fibers, Cellulose Ethers, Cellulose Esters, Microcrystalline Cellulose, Nanocellulose, and Others), By End-Use Industry (Textile, Food, Chemical Synthesis, Pharmaceuticals, Construction, Paper & Pulp, Paints & Coatings, and Others), and Regional Forecast, 2019-2026*; 2020.
74. Morán, J. I.; Alvarez, V. A.; Cyras, V. P.; Vázquez, A., Extraction of cellulose and preparation of nanocellulose from sisal fibers. *Cellulose* **2007,** *15* (1), 149-159.
75. Mandal, A.; Chakrabarty, D., Isolation of nanocellulose from waste sugarcane bagasse (SCB) and its characterization. *Carbohydrate Polymers* **2011,** *86* (3), 1291-1299.
76. Dufresne, A., Nanocellulose: a new ageless bionanomaterial. *Materials Today* **2013,** *16* (6), 220-227.
77. Lin, N.; Dufresne, A., Nanocellulose in biomedicine: Current status and future prospect. *European Polymer Journal* **2014,** *59*, 302-325.
78. Jorfi, M.; Foster, E. J., Recent advances in nanocellulose for biomedical applications. *Journal of Applied Polymer Science* **2015,** *132* (14), n/a-n/a.
79. Abitbol, T.; Rivkin, A.; Cao, Y.; Nevo, Y.; Abraham, E.; Ben-Shalom, T.; Lapidot, S.; Shoseyov, O., Nanocellulose, a tiny fiber with huge applications. *Curr Opin Biotechnol* **2016,** *39*, 76-88.
80. Klemm, D.; Heublein, B.; Fink, H. P.; Bohn, A., Cellulose: fascinating biopolymer and sustainable raw material. *Angew Chem Int Ed Engl* **2005,** *44* (22), 3358-93.
81. Habibi, Y.; Lucia, L. A.; Rojas, O. J., Cellulose Nanocrystals: Chemistry, Self-Assembly, and Applications. *Chemical Reviews* **2010,** *110*, 3479–3500.
82. George, J.; Sabapathi, S. N., Cellulose nanocrystals: synthesis, functional properties, and applications. *Nanotechnol Sci Appl* **2015,** *8*, 45-54.
83. Tang, L. R.; Huang, B.; Ou, W.; Chen, X. R.; Chen, Y. D., Manufacture of cellulose nanocrystals by cation exchange resin-catalyzed hydrolysis of cellulose. *Bioresour Technol* **2011,** *102* (23), 10973-7.
84. Camarero Espinosa, S.; Kuhnt, T.; Foster, E. J.; Weder, C., Isolation of thermally stable cellulose nanocrystals by phosphoric acid hydrolysis. *Biomacromolecules* **2013,** *14* (4), 1223-30.
85. Santos, R. M. d.; Flauzino Neto, W. P.; Silvério, H. A.; Martins, D. F.; Dantas, N. O.; Pasquini, D., Cellulose nanocrystals from pineapple leaf, a new approach for the reuse of this agro-waste. *Industrial Crops and Products* **2013,** *50*, 707-714.
86. Yu, H.-Y.; Zhang, D.-Z.; Lu, F.-F.; Yao, J., New Approach for Single-Step Extraction of Carboxylated Cellulose Nanocrystals for Their Use As Adsorbents and Flocculants. *ACS Sustainable Chemistry & Engineering* **2016,** *4* (5), 2632-2643.

87. Vasconcelos, N. F.; Feitosa, J. P.; da Gama, F. M.; Morais, J. P.; Andrade, F. K.; de Souza Filho, M. S.; Rosa, M. F., Bacterial cellulose nanocrystals produced under different hydrolysis conditions: Properties and morphological features. *Carbohydr Polym* **2017,** *155*, 425-431.
88. Zhang, K.; Sun, P.; Liu, H.; Shang, S.; Song, J.; Wang, D., Extraction and comparison of carboxylated cellulose nanocrystals from bleached sugarcane bagasse pulp using two different oxidation methods. *Carbohydr Polym* **2016,** *138*, 237-43.
89. Zhou, Y.; Saito, T.; Bergstrom, L.; Isogai, A., Acid-Free Preparation of Cellulose Nanocrystals by TEMPO Oxidation and Subsequent Cavitation. *Biomacromolecules* **2018,** *19* (2), 633-639.
90. Li, W.; Yue, J.; Liu, S., Preparation of nanocrystalline cellulose via ultrasound and its reinforcement capability for poly(vinyl alcohol) composites. *Ultrason Sonochem* **2012,** *19* (3), 479-85.
91. Li, Y.; Liu, Y.; Chen, W.; Wang, Q.; Liu, Y.; Li, J.; Yu, H., Facile extraction of cellulose nanocrystals from wood using ethanol and peroxide solvothermal pretreatment followed by ultrasonic nanofibrillation. *Green Chemistry* **2016,** *18* (4), 1010-1018.
92. Dufresne, A., *Nanocellulose: from nature to high performance tailored materials*. Walter de Gruyter GmbH & Co KG: 2017.
93. Araki, J.; Wada, M.; Kuga, S., Steric stabilization of a cellulose microcrystal suspension by poly (ethylene glycol) grafting. *Langmuir* **2001,** *17* (1), 21-27.
94. Beck-Candanedo, S.; Roman, M.; Gray, D., Effect of Reaction Conditions on the Properties and Behavior of Wood Cellulose Nanocrystal Suspensions. *Biomacromolecules* **2005,** *6*, 1048-1054.
95. Pranger, L.; Tannenbaum, R., Biobased Nanocomposites Prepared by In Situ Polymerization of Furfuryl Alcohol with Cellulose Whiskers or Montmorillonite Clay. *Macromolecules* **2008,** *41*, 8682-8687.
96. Capadona, J. R.; Shanmuganathan, K.; Trittschuh, S.; Seidel, S.; Rowan, S. J.; Weder, C., Polymer Nanocomposites with Nanowhiskers Isolated from Microcrystalline Cellulose. *Biomacromolecules* **2009,** *10*, 712–716.
97. De Menezes, A. J.; Siqueira, G.; Curvelo, A. A.; Dufresne, A., Extrusion and characterization of functionalized cellulose whiskers reinforced polyethylene nanocomposites. *Polymer* **2009,** *50* (19), 4552-4563.
98. Peng, B. L.; Dhar, N.; Liu, H. L.; Tam, K. C., Chemistry and applications of nanocrystalline cellulose and its derivatives: A nanotechnology perspective. *The Canadian Journal of Chemical Engineering* **2011,** *89* (5), 1191-1206.
99. George, J.; Bawa, A. S. In *Synthesis and characterization of bacterial cellulose nanocrystals and their PVA nanocomposites*, Advanced Materials Research, Trans Tech Publ: 2010; pp 383-386.
100. George, J., High performance edible nanocomposite films containing bacterial cellulose nanocrystals. *Carbohydrate Polymers* **2012,** *87* (3), 2031-2037.
101. Tang, J.; Sisler, J.; Grishkewich, N.; Tam, K. C., Functionalization of cellulose nanocrystals for advanced applications. *J Colloid Interface Sci* **2017,** *494*, 397-409.
102. Rahaman, M.; Aldalbahi, A.; Govindasami, P.; Khanam, N. P.; Bhandari, S.; Feng, P.; Altalhi, T., A New Insight in Determining the Percolation Threshold of Electrical Conductivity for Extrinsically Conducting Polymer Composites through Different Sigmoidal Models. *Polymers (Basel)* **2017,** *9* (10).

103. Ram, R.; Rahaman, M.; Aldalbahi, A.; Khastgir, D., Determination of percolation threshold and electrical conductivity of polyvinylidene fluoride (PVDF)/short carbon fiber (SCF) composites: effect of SCF aspect ratio. *Polymer International* **2017,** *66* (4), 573-582.
104. Han, J.; Wang, H.; Yue, Y.; Mei, C.; Chen, J.; Huang, C.; Wu, Q.; Xu, X., A self-healable and highly flexible supercapacitor integrated by dynamically cross-linked electro-conductive hydrogels based on nanocellulose-templated carbon nanotubes embedded in a viscoelastic polymer network. *Carbon* **2019,** *149*, 1-18.
105. Hamad, W., On the Development and Applications of Cellulosic Nanofibrillar and Nanocrystalline Materials. *The Canadian Journal of Chemical Engineering* **2006,** *84*, 513-519.
106. Peresin, M. S.; Habibi, Y.; Zoppe, J.; Pawlak, J. J.; Rojas, O. J., Nanofiber Composites of Polyvinyl Alcohol and Cellulose Nanocrystals: Manufacture and Characterization. *Biomacromolecules* **2010,** *11*, 674–681.
107. Xu, X.; Liu, F.; Jiang, L.; Zhu, J. Y.; Haagenson, D.; Wiesenborn, D. P., Cellulose nanocrystals vs. cellulose nanofibrils: a comparative study on their microstructures and effects as polymer reinforcing agents. *ACS Appl Mater Interfaces* **2013,** *5* (8), 2999-3009.
108. Aloui, H.; Khwaldia, K.; Hamdi, M.; Fortunati, E.; Kenny, J. M.; Buonocore, G. G.; Lavorgna, M., Synergistic Effect of Halloysite and Cellulose Nanocrystals on the Functional Properties of PVA Based Nanocomposites. *ACS Sustainable Chemistry & Engineering* **2016,** *4* (3), 794-800.
109. Jahan, Z.; Niazi, M. B. K.; Gregersen, Ø. W., Mechanical, thermal and swelling properties of cellulose nanocrystals/PVA nanocomposites membranes. *Journal of Industrial and Engineering Chemistry* **2018,** *57*, 113-124.
110. Peresin, M. S.; Vesterinen, A.-H.; Habibi, Y.; Johansson, L.-S.; Pawlak, J. J.; Nevzorov, A. A.; Rojas, O. J., Crosslinked PVA nanofibers reinforced with cellulose nanocrystals: Water interactions and thermomechanical properties. *Journal of Applied Polymer Science* **2014,** *131* (11).
111. Tanpichai, S.; Oksman, K., Cross-linked nanocomposite hydrogels based on cellulose nanocrystals and PVA: Mechanical properties and creep recovery. *Composites Part A: Applied Science and Manufacturing* **2016,** *88*, 226-233.
112. Han, L.; Cui, S.; Yu, H. Y.; Song, M.; Zhang, H.; Grishkewich, N.; Huang, C.; Kim, D.; Tam, K. M. C., Self-Healable Conductive Nanocellulose Nanocomposites for Biocompatible Electronic Skin Sensor Systems. *ACS Appl Mater Interfaces* **2019,** *11* (47), 44642-44651.
113. de Rodriguez, N. L. G.; Thielemans, W.; Dufresne, A., Sisal cellulose whiskers reinforced polyvinyl acetate nanocomposites. *Cellulose* **2006,** *13* (3), 261-270.
114. Moon, R. J.; Martini, A.; Nairn, J.; Simonsen, J.; Youngblood, J., Cellulose nanomaterials review: structure, properties and nanocomposites. *Chem Soc Rev* **2011,** *40* (7), 3941-94.
115. Kim, J.-H.; Shim, B. S.; Kim, H. S.; Lee, Y.-J.; Min, S.-K.; Jang, D.; Abas, Z.; Kim, J., Review of nanocellulose for sustainable future materials. *International Journal of Precision Engineering and Manufacturing-Green Technology* **2015,** *2* (2), 197-213.
116. Zhou, T.; Qi, H.; Han, L.; Barbash, D.; Li, C. Y., Towards controlled polymer brushes via a self-assembly-assisted-grafting-to approach. *Nat Commun* **2016,** *7*, 11119.
117. Wu, Y.; Wang, L.; Qing, Y.; Yan, N.; Tian, C.; Huang, Y., A green route to prepare fluorescent and absorbent nano-hybrid hydrogel for water detection. *Sci Rep* **2017,** *7* (1), 4380.
118. Tang, J.; Lee, M. F.; Zhang, W.; Zhao, B.; Berry, R. M.; Tam, K. C., Dual responsive pickering emulsion stabilized by poly[2-(dimethylamino)ethyl methacrylate] grafted cellulose nanocrystals. *Biomacromolecules* **2014,** *15* (8), 3052-60.

119. Wohlhauser, S.; Delepierre, G.; Labet, M.; Morandi, G.; Thielemans, W.; Weder, C.; Zoppe, J. O., Grafting PolymersfromCellulose Nanocrystals: Synthesis, Properties, and Applications. *Macromolecules* **2018,** *51* (16), 6157-6189.
120. Grishkewich, N.; Akhlaghi, S. P.; Zhaoling, Y.; Berry, R.; Tam, K. C., Cellulose nanocrystal-poly(oligo(ethylene glycol) methacrylate) brushes with tunable LCSTs. *Carbohydr Polym* **2016,** *144*, 215-22.
121. Wang, Z.; Zhang, Y.; Yuan, L.; Hayat, J.; Trenor, N. M.; Lamm, M. E.; Vlaminck, L.; Billiet, S.; Du Prez, F. E.; Wang, Z.; Tang, C., Biomass Approach toward Robust, Sustainable, Multiple-Shape-Memory Materials. *ACS Macro Letters* **2016,** *5* (5), 602-606.
122. Yin, Y.; Tian, X.; Jiang, X.; Wang, H.; Gao, W., Modification of cellulose nanocrystal via SI-ATRP of styrene and the mechanism of its reinforcement of polymethylmethacrylate. *Carbohydr Polym* **2016,** *142*, 206-12.
123. Zhang, J.; Wu, Q.; Li, M.-C.; Song, K.; Sun, X.; Lee, S.-Y.; Lei, T., Thermoresponsive Copolymer Poly(N-Vinylcaprolactam) Grafted Cellulose Nanocrystals: Synthesis, Structure, and Properties. *ACS Sustainable Chemistry & Engineering* **2017,** *5* (8), 7439-7447.
124. Zhang, X.; Zhang, J.; Dong, L.; Ren, S.; Wu, Q.; Lei, T., Thermoresponsive poly(poly(ethylene glycol) methylacrylate)s grafted cellulose nanocrystals through SI-ATRP polymerization. *Cellulose* **2017,** *24* (10), 4189-4203.
125. Morandi, G.; Heath, L.; Thielemans, W., Cellulose nanocrystals grafted with polystyrene chains through surface-initiated atom transfer radical polymerization (SI-ATRP). *Langmuir* **2009,** *25* (14), 8280-6.
126. Zoppe, J.; Habibi, Y.; Rojas, O. J.; Venditti, R. A.; Johansson, L. S.; Efimenko, K.; Osterberg, M.; Laine, J., Poly(N-isopropylacrylamide) Brushes Grafted from Cellulose Nanocrystals via Surface-Initiated Single-Electron Transfer Living Radical Polymerization. *Biomacromolecules* **2010,** *11*, 2683–2691.
127. Zhang, Z.; Tam, K. C.; Sebe, G.; Wang, X., Convenient characterization of polymers grafted on cellulose nanocrystals via SI-ATRP without chain cleavage. *Carbohydr Polym* **2018,** *199*, 603-609.
128. Risteen, B.; McBride, M.; Gonzalez, M.; Khau, B.; Zhang, G.; Reichmanis, E., Functionalized Cellulose Nanocrystal-Mediated Conjugated Polymer Aggregation. *ACS Appl Mater Interfaces* **2019,** *11* (28), 25338-25350.
129. Yu, J.; Wang, C.; Wang, J.; Chu, F., In situ development of self-reinforced cellulose nanocrystals based thermoplastic elastomers by atom transfer radical polymerization. *Carbohydr Polym* **2016,** *141*, 143-50.
130. Hatton, F. L.; Kedzior, S. A.; Cranston, E. D.; Carlmark, A., Grafting-from cellulose nanocrystals via photoinduced Cu-mediated reversible-deactivation radical polymerization. *Carbohydr Polym* **2017,** *157*, 1033-1040.
131. Wang, G.; Xi, M.; Bai, L.; Liang, Y.; Yang, L.; Wang, W.; Chen, H.; Yang, H., Pickering emulsion of metal-free photoinduced electron transfer-ATRP stabilized by cellulose nanocrystals. *Cellulose* **2019,** *26* (10), 5947-5957.
132. Morits, M.; McKee, J. R.; Majoinen, J.; Malho, J.-M.; Houbenov, N.; Seitsonen, J.; Laine, J.; Gröschel, A. H.; Ikkala, O., Polymer Brushes on Cellulose Nanofibers: Modification, SI-ATRP, and Unexpected Degradation Processes. *ACS Sustainable Chemistry & Engineering* **2017,** *5* (9), 7642-7650.
133. Abousalman-Rezvani, Z.; Eskandari, P.; Roghani-Mamaqani, H.; Mardani, H.; Salami-Kalajahi, M., Grafting light-, temperature, and CO2-responsive copolymers from cellulose nanocrystals by atom transfer radical polymerization for adsorption of nitrate ions. *Polymer* **2019,** *182*.

134. Risteen, B.; Delepierre, G.; Srinivasarao, M.; Weder, C.; Russo, P.; Reichmanis, E.; Zoppe, J., Thermally Switchable Liquid Crystals Based on Cellulose Nanocrystals with Patchy Polymer Grafts. *Small* **2018,** *14* (46), e1802060.
135. Zoppe, J. O.; Dupire, A. V. M.; Lachat, T. G. G.; Lemal, P.; Rodriguez-Lorenzo, L.; Petri-Fink, A.; Weder, C.; Klok, H.-A., Cellulose Nanocrystals with Tethered Polymer Chains: Chemically Patchy versus Uniform Decoration. *ACS Macro Letters* **2017,** *6* (9), 892-897.
136. Bai, L.; Jiang, X.; Sun, Z.; Pei, Z.; Ma, A.; Wang, W.; Chen, H.; Yang, H.; Yang, L.; Wei, D., Self-healing nanocomposite hydrogels based on modified cellulose nanocrystals by surface-initiated photoinduced electron transfer ATRP. *Cellulose* **2019,** *26* (9), 5305-5319.
137. Zhang, Z.; Wang, X.; Tam, K. C.; Sebe, G., A comparative study on grafting polymers from cellulose nanocrystals via surface-initiated atom transfer radical polymerization (ATRP) and activator re-generated by electron transfer ATRP. *Carbohydr Polym* **2019,** *205*, 322-329.
138. Zhang, Z.; Sebe, G.; Wang, X.; Tam, K. C., Gold nanoparticles stabilized by poly(4-vinylpyridine) grafted cellulose nanocrystals as efficient and recyclable catalysts. *Carbohydr Polym* **2018,** *182*, 61-68.
139. Hansson, S.; Carlmark, A.; Malmström, E.; Fogelström, L., Toward industrial grafting of cellulosic substrates via ARGET ATRP. *Journal of Applied Polymer Science* **2015,** *132* (6), n/a-n/a.
140. Zhao, B.; Brittain, W. J., Polymer brushes: surface-immobilized macromolecules. *Progress in Polymer Science* **2000,** *25* (5), 677-710.
141. Tou, F.; Yang, Y.; Feng, J.; Niu, Z.; Pan, H.; Qin, Y.; Guo, X.; Meng, X.; Liu, M.; Hochella, M. F., Environmental Risk Implications of Metals in Sludges from Waste Water Treatment Plants: The Discovery of Vast Stores of Metal-Containing Nanoparticles. *Environ Sci Technol* **2017,** *51* (9), 4831-4840.
142. Tsang, M. P.; Hristozov, D.; Zabeo, A.; Koivisto, A. J.; Jensen, A. C. O.; Jensen, K. A.; Pang, C.; Marcomini, A.; Sonnemann, G., Probabilistic risk assessment of emerging materials: case study of titanium dioxide nanoparticles. *Nanotoxicology* **2017,** *11* (4), 558-568.
143. Drogat, N.; Granet, R.; Sol, V.; Memmi, A.; Saad, N.; Klein Koerkamp, C.; Bressollier, P.; Krausz, P., Antimicrobial silver nanoparticles generated on cellulose nanocrystals. *Journal of Nanoparticle Research* **2010,** *13* (4), 1557-1562.
144. Azizi, S.; Ahmad, M. B.; Hussein, M. Z.; Ibrahim, N. A., Synthesis, antibacterial and thermal studies of cellulose nanocrystal stabilized ZnO-Ag heterostructure nanoparticles. *Molecules* **2013,** *18* (6), 6269-80.
145. Yu, H.-Y.; Qin, Z.-Y.; Sun, B.; Yan, C. F.; Yao, J.-M., One-pot green fabrication and antibacterial activity of thermally stable corn-like CNC/Ag nanocomposites. *Journal of Nanoparticle Research* **2013,** *16* (1).
146. Yu, H.-Y.; Chen, G.-Y.; Wang, Y.-B.; Yao, J.-M., A facile one-pot route for preparing cellulose nanocrystal/zinc oxide nanohybrids with high antibacterial and photocatalytic activity. *Cellulose* **2014,** *22* (1), 261-273.
147. Yang, R.-T.; Yu, H.-Y.; Song, M.-L.; Zhou, Y.-W.; Yao, J.-M., Flower-like zinc oxide nanorod clusters grown on spherical cellulose nanocrystals via simple chemical precipitation method. *Cellulose* **2016,** *23* (3), 1871-1884.
148. Dong, Y.-Y.; Liu, S.; Liu, Y.-J.; Meng, L.-Y.; Ma, M.-G., Ag@Fe3O4@cellulose nanocrystals nanocomposites: microwave-assisted hydrothermal synthesis, antimicrobial properties, and good adsorption of dye solution. *Journal of Materials Science* **2017,** *52* (13), 8219-8230.
149. Wang, S.; Sun, J.; Jia, Y.; Yang, L.; Wang, N.; Xianyu, Y.; Chen, W.; Li, X.; Cha, R.; Jiang, X., Nanocrystalline Cellulose-Assisted Generation of Silver Nanoparticles for Nonenzymatic Glucose Detection and Antibacterial Agent. *Biomacromolecules* **2016,** *17* (7), 2472-8.

150. Shaheen, T. I.; Fouda, A., Green approach for one-pot synthesis of silver nanorod using cellulose nanocrystal and their cytotoxicity and antibacterial assessment. *Int J Biol Macromol* **2018,** *106*, 784-792.
151. Chen, L.; Yu, H.; Deutschman, C.; Yang, T.; Tam, K. C., Novel design of Fe-Cu alloy coated cellulose nanocrystals with strong antibacterial ability and efficient Pb(2+) removal. *Carbohydr Polym* **2020,** *234*, 115889.
152. de Castro, D. O.; Bras, J.; Gandini, A.; Belgacem, N., Surface grafting of cellulose nanocrystals with natural antimicrobial rosin mixture using a green process. *Carbohydrate Polymers* **2016,** *137*, 1-8.
153. Tang, J.; Song, Y.; Tanvir, S.; Anderson, W. A.; Berry, R. M.; Tam, K. C., Polyrhodanine Coated Cellulose Nanocrystals: A Sustainable Antimicrobial Agent. *ACS Sustainable Chemistry & Engineering* **2015,** *3* (8), 1801-1809.
154. Tavakolian, M.; Jafari, S. M.; van de Ven, T. G. M., A Review on Surface-Functionalized Cellulosic Nanostructures as Biocompatible Antibacterial Materials. *Nano-Micro Letters* **2020,** *12* (1).
155. Saini, S.; Yucel Falco, C.; Belgacem, M. N.; Bras, J., Surface cationized cellulose nanofibrils for the production of contact active antimicrobial surfaces. *Carbohydr Polym* **2016,** *135*, 239-47.
156. Belkhir, K.; Lacroix, M.; Jamshidian, M.; Salmieri, S.; Jegat, C.; Taha, M., Evaluation of antibacterial activity of branched quaternary ammonium grafted green polymers. *Food Packaging and Shelf Life* **2017,** *12*, 28-41.
157. Bespalova, Y.; Kwon, D.; Vasanthan, N., Surface modification and antimicrobial properties of cellulose nanocrystals. *Journal of Applied Polymer Science* **2017,** *134* (18).
158. Liu, Y.; Li, M.; Qiao, M.; Ren, X.; Huang, T.-S.; Buschle-Diller, G., Antibacterial membranes based on chitosan and quaternary ammonium salts modified nanocrystalline cellulose. *Polymers for Advanced Technologies* **2017,** *28* (12), 1629-1635.
159. Li, M.; Liu, X.; Liu, N.; Guo, Z.; Singh, P. K.; Fu, S., Effect of surface wettability on the antibacterial activity of nanocellulose-based material with quaternary ammonium groups. *Colloids and Surfaces A: Physicochemical and Engineering Aspects* **2018,** *554*, 122-128.
160. Lu, S.; Tang, Z.; Li, W.; Ouyang, X.; Cao, S.; Chen, L.; Huang, L.; Wu, H.; Ni, Y., Diallyl dimethyl ammonium chloride-grafted cellulose filter membrane via ATRP for selective removal of anionic dye. *Cellulose* **2018,** *25* (12), 7261-7275.
161. Wessels, S.; Ingmer, H., Modes of action of three disinfectant active substances: a review. *Regul Toxicol Pharmacol* **2013,** *67* (3), 456-67.
162. Jennings, M. C.; Minbiole, K. P.; Wuest, W. M., Quaternary Ammonium Compounds: An Antimicrobial Mainstay and Platform for Innovation to Address Bacterial Resistance. *ACS Infect Dis* **2015,** *1* (7), 288-303.
163. Zhang, C.; Cui, F.; Zeng, G. M.; Jiang, M.; Yang, Z. Z.; Yu, Z. G.; Zhu, M. Y.; Shen, L. Q., Quaternary ammonium compounds (QACs): a review on occurrence, fate and toxicity in the environment. *Sci Total Environ* **2015,** *518-519*, 352-62.
164. de Oliveira Pedro, R.; Schmitt, C. C.; Neumann, M. G., Syntheses and characterization of amphiphilic quaternary ammonium chitosan derivatives. *Carbohydr Polym* **2016,** *147*, 97-103.
165. Makvandi, P.; Jamaledin, R.; Jabbari, M.; Nikfarjam, N.; Borzacchiello, A., Antibacterial quaternary ammonium compounds in dental materials: A systematic review. *Dent Mater* **2018,** *34* (6), 851-867.
166. Li, F.; Weir, M.; Xu, H., Effects of quaternary ammonium chain length on antibacterial bonding agents. *Journal of dental research* **2013,** *92* (10), 932-938.

167. Zhou, H.; Li, F.; Weir, M. D.; Xu, H. H., Dental plaque microcosm response to bonding agents containing quaternary ammonium methacrylates with different chain lengths and charge densities. *J Dent* **2013,** *41* (11), 1122-31.
168. Liang, X.; Soderling, E.; Liu, F.; He, J.; Lassila, L. V.; Vallittu, P. K., Optimizing the concentration of quaternary ammonium dimethacrylate monomer in bis-GMA/TEGDMA dental resin system for antibacterial activity and mechanical properties. *J Mater Sci Mater Med* **2014,** *25* (5), 1387-93.
169. Xu, X.; Wang, Y.; Liao, S.; Wen, Z. T.; Fan, Y., Synthesis and characterization of antibacterial dental monomers and composites. *J Biomed Mater Res B Appl Biomater* **2012,** *100* (4), 1151-62.
170. Sharma, V. K.; Johnson, N.; Cizmas, L.; McDonald, T. J.; Kim, H., A review of the influence of treatment strategies on antibiotic resistant bacteria and antibiotic resistance genes. *Chemosphere* **2016,** *150*, 702-714.
171. Tacconelli, E.; Carrara, E.; Savoldi, A.; Harbarth, S.; Mendelson, M.; Monnet, D. L.; Pulcini, C.; Kahlmeter, G.; Kluytmans, J.; Carmeli, Y., Discovery, research, and development of new antibiotics: the WHO priority list of antibiotic-resistant bacteria and tuberculosis. *The Lancet Infectious Diseases* **2018,** *18* (3), 318-327.
172. Jiao, Y.; Niu, L. N.; Ma, S.; Li, J.; Tay, F. R.; Chen, J. H., Quaternary ammonium-based biomedical materials: State-of-the-art, toxicological aspects and antimicrobial resistance. *Prog Polym Sci* **2017,** *71*, 53-90.
173. Elena, P.; Miri, K., Formation of contact active antimicrobial surfaces by covalent grafting of quaternary ammonium compounds. *Colloids Surf B Biointerfaces* **2018,** *169*, 195-205.
174. McBain, A.; Rickard, A.; Gilbert, P., Possible implications of biocide accumulation in the environment on the prevalence of bacterial antibiotic resistance. *Journal of Industrial Microbiology and Biotechnology* **2002,** *29* (6), 326-330.
175. Hegstad, K.; Langsrud, S.; Lunestad, B. T.; Scheie, A. A.; Sunde, M.; Yazdankhah, S. P., Does the wide use of quaternary ammonium compounds enhance the selection and spread of antimicrobial resistance and thus threaten our health? *Microbial drug resistance* **2010,** *16* (2), 91-104.
176. Buffet-Bataillon, S.; Tattevin, P.; Bonnaure-Mallet, M.; Jolivet-Gougeon, A., Emergence of resistance to antibacterial agents: the role of quaternary ammonium compounds--a critical review. *Int J Antimicrob Agents* **2012,** *39* (5), 381-9.
177. Druvari, D.; Koromilas, N.; Bekiari, V.; Bokias, G.; Kallitsis, J., Polymeric Antimicrobial Coatings Based on Quaternary Ammonium Compounds. *Coatings* **2017,** *8* (1).
178. Zubris, D. L.; Minbiole, K. P. C.; Wuest, W. M., Polymeric Quaternary Ammonium Compounds: Versatile Antimicrobial Materials. *Current Topics in Medicinal Chemistry* **2017,** *17*, 305-318.
179. Muñoz-Bonilla, A.; Fernández-García, M., Polymeric materials with antimicrobial activity. *Progress in Polymer Science* **2012,** *37* (2), 281-339.
180. Cho, K.-H.; Park, J.-E.; Osaka, T.; Park, S.-G., The study of antimicrobial activity and preservative effects of nanosilver ingredient. *Electrochimica Acta* **2005,** *51* (5), 956-960.
181. Eyley, S.; Thielemans, W., Surface modification of cellulose nanocrystals. *Nanoscale* **2014,** *6* (14), 7764-79.
182. Xiong, R.; Lu, C.; Zhang, W.; Zhou, Z.; Zhang, X., Facile synthesis of tunable silver nanostructures for antibacterial application using cellulose nanocrystals. *Carbohydr Polym* **2013,** *95* (1), 214-9.

183. Singla, R.; Soni, S.; Kulurkar, P. M.; Kumari, A.; S, M.; Patial, V.; Padwad, Y. S.; Yadav, S. K., In situ functionalized nanobiocomposites dressings of bamboo cellulose nanocrystals and silver nanoparticles for accelerated wound healing. *Carbohydr Polym* **2017,** *155*, 152-162.
184. Feese, E.; Sadeghifar, H.; Gracz, H. S.; Argyropoulos, D. S.; Ghiladi, R. A., Photobactericidal porphyrin-cellulose nanocrystals: synthesis, characterization, and antimicrobial properties. *Biomacromolecules* **2011,** *12* (10), 3528-39.
185. Poverenov, E.; Shemesh, M.; Gulino, A.; Cristaldi, D. A.; Zakin, V.; Yefremov, T.; Granit, R., Durable contact active antimicrobial materials formed by a one-step covalent modification of polyvinyl alcohol, cellulose and glass surfaces. *Colloids and Surfaces B: Biointerfaces* **2013,** *112*, 356-361.
186. Li, M.; Fu, S., Functionally Modified Cellulose Nanocrystals as an Adsorbent for Anionic Dyes. *Paper and Biomaterials* **2018,** *3*, 1.
187. Arredondo, J.; Jessop, P. G.; Champagne, P.; Bouchard, J.; Cunningham, M. F., Synthesis of CO2-responsive cellulose nanocrystals by surface-initiated Cu(0)-mediated polymerisation. *Green Chemistry* **2017,** *19* (17), 4141-4152.
188. Rinkenauer, A. C.; Schallon, A.; Gunther, U.; Wagner, M.; Betthausen, E.; Schubert, U. S.; Schacher, F. S., A Paradigm Change: Efficient Transfection of Human Leukemia Cells by Stimuli-Responsive Multicompartment Micelles. *ACS Nano* **2013,** *7*, 9621–9631.
189. Majewski, A. P.; Stahlschmidt, U.; Jerome, V.; Freitag, R.; Muller, A. H.; Schmalz, H., PDMAEMA-grafted core-shell-corona particles for nonviral gene delivery and magnetic cell separation. *Biomacromolecules* **2013,** *14* (9), 3081-90.
190. Lin, N.; Dufresne, A., Surface chemistry, morphological analysis and properties of cellulose nanocrystals with gradiented sulfation degrees. *Nanoscale* **2014,** *6* (10), 5384-93.